UNIVERSITY OF CALIFORNIA,
IRVINE

Molecular properties within the generalized Kohn–Sham random phase approximation

DISSERTATION

submitted in partial satisfaction of the requirements
for the degree of

DOCTOR OF PHILOSOPHY

in Chemistry

by

Sree Ganesh Balasubramani

Dissertation Committee:
Professor Filipp Furche, Chair
Professor Kieron Burke
Professor Ioan Andricioaei

2019

DEDICATION

To Amma, Appa, Pappa and Soma.

TABLE OF CONTENTS

LIST OF FIGURES

LIST OF TABLES

ACKNOWLEDGMENTS

First and foremost I would like to thank my mother, father, sister and wife for their unlimited supply of love and support which fueled me for the past six years. My father and mother are the most hardworking people that I know of, and they have sacrificed so much for me to do well in life and I am thankful for that. My little sister has constantly inspired me with her fresh perspectives on life and served as an example for being free spirited and to follow your dreams and I thank her for showing me that.

My wife Soma, has been an incredible source of strength for me. Soma has cheered me up when I was down and listened to all my grievances with patience. It is next to impossible for me to have been through graduate life without her love and support, and I am endlessly thankful to her for all that she has done for me.

Filipp has always given me insightful advice and taught me to think about problems from very different perspectives both in quantum chemistry and in life. I am thankful for the conversations he has had with me over the past six years, helping me learn about self motivation and teaching me a lot of things that cannot be obtained from reading books or papers. I have learned how to be organized, meticulous, rigorous and develop several tools for monitoring progress which are valuable in any walk of life and I am thankful to him for teaching me these.

Vamsee was my co-advisor for the first four years, helping me understand the hard work and dedication that is required to work on cutting-edge research problems. He became a good friend and mentor, an excellent office mate and I am thankful to him for his constant encouragement that motivated me to work hard and solve problems. I thank Shane for teaching me to be a true professional while having a lot of fun and sharing an office with him was a great experience. Shane has helped me with coding, quantum chemistry, TURBOMOLE, slack lining. Guo was an excellent senior and a incredibly knowledgeable coworker who was willing to share his ideas with me and I thank him for teaching me the importance of rigor in theoretical chemistry. I thank all the Furche group members that I had the opportunity to meet and discuss science, they have all helped in one way or another to progress with different projects.

I thank Prof. Kieron Burke, who was in my dissertation and advancement exam committees, helped me navigate the density functional theory world with his excellent courses. Prof. Ioan Andricioaei helped me learn thermodynamics and non-equilibrium statistical mechanics and was part of my dissertation committee and I thank him for his help.

Saswata and me often found ourselves going through the same problems during our PhD and we have always helped each other by just having long conversations about these problems. I am thankful to have Saswata as a great friend and coworker. My time here was also made fun by a lot of friends, Anupam, Saleh, Karissa, Apurva, Nihesh, Srikiran, Yash and many others and I am grateful to them. I am thankful to Ankitha and Bhupalee for all the lunchtime conversations and Wholesome choice trips over the last year.

This material is based upon work supported by the National Science Foundation under CHE−1213382, CHE−1464828 and CHE−1800431.

VITA

Sree Ganesh Balasubramani

EDUCATION

Doctor of Philosophy in Chemistry **2020**
University of California *Irvine, California, USA*

Dual degree Bachelor-Master of Science **2014**
Indian Institute of Science Education and Research *Thiruvananthapuram, Kerala, India*

REFEREED JOURNAL PUBLICATIONS

Variational generalized Kohn-Sham approach combining the random-phase-approximation and Green's-function methods **2019**
V. K. Voora, S. G. Balasubramani, F. Furche

Phys. Rev. A **99**, 012518 (2019)

Synthesis, Structure, and Magnetism of Tris(amide) [Ln{N(SiMe$_3$)$_2$}$_3$] **2018**
A. J. Ryan, L. E. Dalgarno, S. G. Balasubramani, G. P. Chen, J. W. Ziller, F. Furche, J. R. Long, W. J. Evans

Chem.: Eur. J. **24**, 7702 (2018)

Random-Phase Approximation Methods **2017**
G. P. Chen, V. K. Voora, M. Agee, S. G. Balasubramani, F. Furche

Annu. Rev. Phys. Chem. **68**, 421 (2017)

Noble gas encapsulation into carbon nanotubes: Predictions from analytical model and DFT studies **2014**
S. G. Balasubramani, D. Singh, R. S. Swathi

J. Chem. Phys. **141**, 184304 (2014)

Poster Presentations

Implementation of analytical static polarizabilities within the random phase approximation **May 2019**
4^{th} Southern California Theoretical Chemistry Symposium

Los Angeles, USA

Second order molecular properties from the random phase approximation **July 2017**
American Conference on Theoretical Chemistry (ACTC)

Boston, USA

Second order molecular properties within the random phase approximation **May 2017**
2^{nd} Southern California Theoretical Chemistry Symposium

Irvine, USA

Analytical second order properties within the RPA **June 2016**
1^{st} Southern California Theoretical Chemistry Symposium

San Diego, USA

Non-covalent interactions using orbital optimized random phase approximation (oRPA) **February 2016**
Computers in chemistry, 251st American Chemical Society National Meeting and Exposition

San Diego, USA

TEACHING EXPERIENCE

Computational Chemistry Laboratory (CHEM 150L) **Winter 2018**
University of California *Irvine, California, USA*

Density Functional Theory (CHEM 252) **Winter 2017**
University of California *Irvine, California, USA*

Computational Chemistry Laboratory (CHEM 231) **Spring 2016**
University of California *Irvine, California, USA*

General Chemistry Laboratory for Engineers (CHEM 1LE) **Winter 2016**
University of California *Irvine, California, USA*

General Chemistry Laboratory (CHEM 1LC) **Spring 2015**
University of California *Irvine, California, USA*

General Chemistry Lecture (CHEM 1A) **Winter 2015**
University of California *Irvine, California, USA*

General Chemistry Laboratory (CHEM 1LD) **Fall 2014**
University of California *Irvine, California, USA*

ABSTRACT OF THE DISSERTATION

Molecular properties within the generalized Kohn–Sham random phase approximation

By

Sree Ganesh Balasubramani

Doctor of Philosophy in Chemistry

University of California, Irvine, 2019

Professor Filipp Furche, Chair

Theoretical calculations of molecular properties can assist experimental design of molecules with interesting optical, electronic and structural properties which would help accelerate materials discovery. Density functional theory (DFT) within the Kohn–Sham (KS) framework has been the most widely used method for molecular properties calculations in the last three decades because of its advantageous computational cost-to-accuracy ratio. However, commonly used density functional approximations (DFAs) have been shown to be inadequate for calculations involving transition metal compounds, metal clusters, conjugated molecules and for describing noncovalent interactions. Random phase approximation is a post-KS DFA that is accurate for describing noncovalent interactions without the need for empirical parameters, does not diverge for small-, or even zero-gap systems and incorporates Hartree–Fock (HF) exchange. The first part of this thesis aims at answering the question: can a self-consistent generalized KS scheme be developed for the RPA energy functional which also gives access to single particle energies within a variational Lagrangian formalism? To this end, an orbital self-consistent scheme called the generalized KS semicanonical projected RPA (GKS-spRPA) is developed, implemented and benchmarked for ground state as well as single particle energies. The ionization energies and band-gaps that are calculated using the GKS-spRPA suggest that it is better than the commonly used G_0W_0 method. The second part of the thesis is concerned with the implementation and testing of static polar-

izabilities ($\boldsymbol{\alpha}(0)$) within the GKS-spRPA method. The GKS-spRPA successfully solves the overpolarization problem observed with the use of semilocal/hybrid DFAs for calculations of $\boldsymbol{\alpha}(0)$ of $\pi-$conjugated molecules. Calculations involving metallocenes, metal clusters and a small molecule testset are used to show that the $\boldsymbol{\alpha}(0)$ calculated using the GKS-spRPA method is more accurate than DFAs such as PBE, PBE0, CAM-B3LYP and wave function based methods such as HF and the second-order Møller–Plesset perturbation theory (MP2). Thus, this thesis conclusively shows that the GKS-spRPA within a Lagrangian framework, is a method that provides not only accurate ground state energies but also a wide range of molecular properties such as geometries, ionization potentials, electron affinities, dipoles and polarizabilities with a reasonable computational cost of $\mathcal{O}(N^4 \log(N))$.

Chapter 1

Background and Theory

 This material is based upon work supported by the National Science Foundation under CHE−1213382 and CHE−1464828.

1.1 Introduction

Chemists have developed various experimental techniques based on probing molecules using electromagnetic radiation to understand their electronic structure and properties in great detail. [1] Often these experimental measurements produce complicated results that can be difficult to interpret especially for larger molecules. Quantum chemical calculations can provide useful insights to understanding these results in such cases. [2] In quantum chemistry and condensed matter physics the method of choice for electronic structure calculations has been density functional theory (DFT) for the past three decades [3, 4]. Specifically, exchange-correlation (XC) functionals developed within the (generalized) Kohn–Sham ((G)KS) scheme [5] such as the local density approximation (LDA) [6], generalized gradient approximation (GGA) [7], meta-GGA (mGGA) [8], hybrid functionals [9, 10] have provided reasonable accuracy at a very cheap computational cost that has led to the widespread use of DFT.

With a plethora of density functional approximations (DFAs) available at a users disposal, the question of which functional to use for a particular molecular system and property of interest can often be difficult to answer [11]. Benchmark calculations can provide some guidelines to answer this question. [12, 13] Using such benchmarks and other extensive studies certain cases have been identified where semilocal (SL) [7] and hybrid [9] DFAs perform erroneously. These problematic cases arise mainly because of self-interaction error which results in non-zero correlation energies for one-electron systems within SL/hybrid DFT [14], lack of long-range correlations that result in poor descriptions of van der Waals interactions [15], exponential decay of the SL KS potential that results in unbound anions [16] and overpolarization of charge density due to lack of field counteracting terms in the KS potential that results in qualitatively wrong electrical response properties [17]. Recent density functional development has been focused on addressing some of these problems as well as satisfaction of other physically motivated exact conditions [18].

Approximate functionals based on the adiabatic connection fluctuation dissipation theorem (ACFDT) such as the random phase approximation (RPA) provide an alternative to SL/hybrid functionals [19]. RPA was originally developed by Bohm and Pines [20, 21] for the description of the ground state energy of the uniform electron gas in the 1950s. Gell-Mann and Brueckner showed that the correlation energy of the electron gas in the high density limit is obtained as the summation of ring type diagrams to all orders and that it was equivalent to the RPA [22]. McLachlan and Ball showed that the time-dependent Hartree–Fock theory (TDHF) and the RPA with exchange (RPAX) are equivalent [23] paving the way for developments of methods to calculate the excitation energies and oscillator strengths of molecules such as the equation-of-motion method [24, 25] and polarization propagator theory [26, 27]. As a post-KS method, ACFDT-DFT was developed by Langreth and Perdew [28] and by Gunnarson and Lundqvist [29]. The simplest approximate functional within the ACFDT is the RPA. Within the post-KS framework RPA is a parameter-free XC energy functional that contains HF exchange while seamlessly including van der Waals interactions [30].

Post-KS RPA was first implemented and tested for molecules using finite basis sets in 2001 by Furche [31]. Since then, RPA has gained prominence in quantum chemistry and solid state physics [32–34]. Efficient implementation of the post-KS RPA within the resolution of identity (RI) approximation (RIRPA) and imaginary frequency integration using quadratures result in a computational scaling of $\mathcal{O}(N^4 \log(N))$ [35], with system size N, compared to the $\mathcal{O}(N^5)$ scaling for second-order Møller-Plesset (MP2) perturbation theory [36, 37]. The RPA correlation energy is not divergent for small- and zero-gap systems unlike perturbative methods such as the MP2 and hence, it can be used for a wide range of systems starting from small molecules to extended systems. Even though long- and medium-range interactions are captured by RPA, short-range correlation effects seem to be poorly described by it [38]. Several remedies have been proposed to address the lack of short-range correlation such as the short-range GGA correction to the RPA correlation energy by Yan et al. [39] RPA suffers from self-correlation errors due to the absence of higher-order exchange terms in the RPA

correlation energy, but methods such as the second-order screened exchange [40, 41] and the approximate exchange kernel [42] can alleviate this issue to various degrees.

First-order properties such as geometrical gradients and dipole moments within RIRPA were implemented and tested by Burow et al. [43], who found that the RIRPA molecular structures were significantly improved compared to MP2, particularly for small-gap systems. Burow et al. calculated numerical second-order properties such as harmonic frequencies using their implementation and found that the RIRPA was more accurate compared to PBE0 and MP2 for a testset of small molecules. Numerical finite differences are often simple to implement but can be prone to numerical instabilities and are not very resource efficient. Analytical energy derivative techniques on the other hand require considerable programming effort but have better precision, accuracy and convenience since they are a direct method for calculating properties [44, 45].

The goal of this thesis is to develop and implement a self-consistent orbital optimization scheme for the RIRPA energy functional using a variational Lagrangian formalism and to benchmark its accuracy for ground state energies as well as first-order properties such as geometrical gradients and quasiparticle energies. Furthermore second-order properties such as the static polarizabilities are to be derived, implemented and tested for the self-consistent RPA energy functional.

The organization of the thesis is as follows. Chapter 1 introduces the variational Lagrangian formalism for the calculation of first-order properties within the RIRPA. The implementation of the RIRPA gradients is extended for unrestricted KS references and its accuracy is bench marked using a set of open-shell molecules. Chapter 2 is regarding the development of the orbital self-consistent generalized KS formalism for the RIRPA energy functional, called the generalized KS semicanonical projected RPA (GKS-spRPA). Thorough analysis of the errors made by GKS-spRPA compared to the post-KS RPA are carried out. The implementation of quasiparticle energies is discussed in detail along with results of band gaps and ioniza-

tion potentials of molecules and molecular ions. Chapter 3 focuses on the derivation and implementation of static polarizabilities within the GKS-spRPA method. Detailed analysis of the implementation is carried out using a variety of molecular systems such as conjugated polymers, metal clusters and organometallic compounds.

1.2 Analytical gradients within RIRPA

Analytical energy gradients are a prerequisite for molecular structure optimization and property calculations [44]. For energies that are variationally determined, their gradients can be efficiently evaluated by virtue of the Hellmann–Feynman theorem. Although the RPA energy functional E RPA is not variational, a Lagrangian can be constructed for computing energy gradients without solving for perturbed KS orbitals [46, 47].

$$\begin{aligned} L^{\mathrm{RPA}}(\mathbf{C},\boldsymbol{\epsilon},\mathbf{D}^{\Delta},\mathbf{W}|\mathbf{h},\mathbf{v},\mathbf{V}^{\mathrm{XC}},\mathbf{S}) = E^{\mathrm{RPA}}(\mathbf{C},\boldsymbol{\epsilon}|\mathbf{h},\mathbf{v}) \\ + \left(\left\langle \mathbf{D}^{\Delta}(\mathbf{C}^{\mathrm{T}}\mathbf{F}\mathbf{C}-\boldsymbol{\epsilon})\right\rangle - \left\langle \mathbf{W}(\mathbf{C}^{\mathrm{T}}\mathbf{S}\mathbf{C}-\mathbf{1})\right\rangle\right). \end{aligned} \tag{1.1}$$

This RPA Lagrangian depends on orbital coefficients $\mathbf{C}$ and a matrix $\boldsymbol{\epsilon}$, that reduces to the diagonal matrix of orbital energies for the input KS solution, as well as on the Lagrange multipliers $\mathbf{D}^{\Delta}$ and $\mathbf{W}$; additionally, L^{RPA} depends parametrically on the one- and two-electron integrals $\mathbf{h}$ and $\mathbf{v}$, the ground-state XC potential matrix $\mathbf{V}^{\mathrm{XC}}$, and the overlap matrix $\mathbf{S}$, all in an atomic orbital (AO) basis. [43]. The Fock matrix $\mathbf{F}$ is the effective one-electron KS Hamiltonian and can be expressed in terms of $\mathbf{h}$, $\mathbf{v}$, and $\mathbf{V}^{\mathrm{XC}}$.

By construction, the correct RPA energy for given KS orbitals and orbital energies is attained by unconstrained optimization of the RPA Lagrangian with respect to $\mathbf{C}$, $\boldsymbol{\epsilon}$, $\mathbf{D}^{\Delta}$ and $\mathbf{W}$.

The variation with respect to $\mathbf{D}^{\Delta}$ enforces that $\mathbf{C}$ and $\boldsymbol{\epsilon}$ satisfy the KS equations

$$\mathbf{C}^{\mathrm{T}}\mathbf{F}\mathbf{C} = \boldsymbol{\epsilon}, \tag{1.2}$$

and the variation with respect to $\mathbf{W}$ recovers the orthonormality constraint

$$\mathbf{C}^{\mathrm{T}}\mathbf{S}\mathbf{C} = \mathbf{1}. \tag{1.3}$$

The corresponding constraint terms in L^{RPA} may be viewed as energetic penalties for violating the constraints, and they both vanish at the stationary point. The total differential of L^{RPA} reveals the physical meaning of the Lagrange multipliers [43]: $\mathbf{D}^{\Delta}$ corresponds to a correction to the KS density matrix $\mathbf{D}^{\mathrm{KS}}$ due to correlation and orbital relaxation, and $\mathbf{W}$ is the energy weighted density matrix [48]. The RPA density matrix

$$\mathbf{D}^{\mathrm{RPA}} = \left.\frac{\mathrm{d}E^{\mathrm{RPA}}}{\mathrm{d}\mathbf{h}}\right|_{stat} = \mathbf{D}^{\mathrm{KS}} + \mathbf{C}\mathbf{D}^{\Delta}\mathbf{C}^{\mathrm{T}} \tag{1.4}$$

facilitates the analysis of RPA calculations in terms of natural orbitals and occupation numbers. Within a spin-restricted formalism, the RPA natural orbitals of stretched H_2 exhibits significant fractional occupation, which resembles the exact solution from coupled-cluster singles and doubles (CCSD) (see Figure 1.1). This result agrees with prior observations that RPA is capable of partially capturing static correlation [31, 49, 50].

The stationarity of the Lagrangian ensures that the orbitals and orbital energies satisfy Wigner's $2n+1$ rule, and the Lagrange multiplies satisfy a stronger $2n+2$ rule [46]. Thus, it is not necessary to solve coupled perturbed KS (CPKS) equations for each perturbation; instead, the Lagrange multipliers can be determined by solving a single set of CPKS equations. With the RI approximation, numerical frequency integration, ERI prescreening techniques, and iterative subspace methods [51, 52], the RPA energy gradient implementation in Turbomole has achieved the same $\mathcal{O}(N^4 \log N)$ scaling as single-point RPA energy calculations.

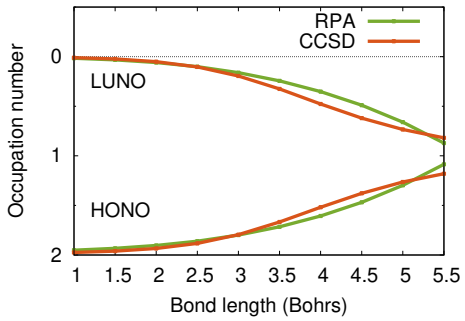

Figure 1.1: Natural orbital occupation numbers of highest occupied natural orbital (HONO) and lowest unoccupied natural orbital (LUNO) of ground-state H_2 using spin-restricted RPA-PBE and CCSD as a function of interatomic distance. aug-cc-pV5Z basis set was used for all computations. An orbital is considered occupied if the occupation is > 1 while it is considered unoccupied if occupation is < 1.

In a typical application, the computational cost for a gradient vector with respect to all nuclear displacements is ~ 5 times that for the corresponding RPA energy. Routine RPA molecular structure optimizations are feasible for systems with ~ 100 atoms using triple- or quadruple-zeta basis sets on single workstation computers [43].

Other recent implementations of RPA analytical gradients [53, 54] are based on the ring-CCD formulation with a HF reference and scales as $\mathcal{O}(N^6)$. Analytic energy gradients were also implemented for range-separated hybrid functionals with short-range semilocal approximation and long-range RPA [54].

1.2.1 Molecular Properties of Radicals

To further assess the performance of RPA, we report the equilibrium structures of a variety of small radicals calculated within RPA for the first time, see Table 1.1. These molecules were selected because accurate experimental bond lengths were available in the literature. Radicals are usually short lived and experimentally elusive intermediates, but single reference methods are often unsuitable for them due to spin contamination and instabilities [55–57]. On the other hand, the RPA structures agree well with experiment, with errors comparable

to closed-shell species [43]. Thus, RPA is a viable approach for computing structures of open shell species. The dependence on the semi-local functional used to generate the KS orbitals is weak, with MAEs of 0.51 pm and 0.56 pm for PBE and TPSS orbitals, respectively.

Table 1.1: Deviations of computed equilibrium bond lengths (pm) of small radicals from experimental reference values; mean absolute deviations (MAEs) are also provided. aug-cc-pV5Z basis sets [58] were used.

	parameter	reference	RPA(TPSS)	RPA(PBE)
OH	O-H	96.97[a]	0.16	0.27
H_2O^+	O-H	100.1[a]	0.02	0.10
HF^+	H-F	100.1[b]	0.40	0.47
NH^+	N-H	107.0[c]	0.28	0.16
HCP^+	H-C	107.3[b]	0.20	0.37
CH_3	C-H	107.67[b]	-0.37	-0.19
N_2^+	N-N	111.642[a]	-0.35	-0.26
CO^+	C-O	112.83[a]	-0.95	-0.82
NO	N-O	115.08[a]	0.42	0.57
CN	C-N	117.18[a]	0.12	0.23
CO_2^+	C-O	117.682[b]	-0.07	0.023
BO	B-O	120.5[a]	0.18	0.31
CF	C-F	127.2[a]	0.44	0.66
F_2^+	F-F	130.5[d]	3.27	3.66
HCP^+	C-P	160.0[b]	-0.39	-0.28
MAE			0.51	0.56

[a]Reference[59], [b]Reference[60], [c]Reference[61], [d]Reference[62]

Although RPA MAEs for the equilibrium bond lengths using the TPSS and PBE functionals are 0.51 pm and 0.56 pm respectively which suggests that the method is accurate for calculations of bond lengths, it needs to be noted that RPA does not always describe the energetics of radicals accurately. [50] For example, consider the potential energy curve (PEC) of H_2^+ [42], which both at the equilibrium bond length as well as at the dissociation length are inaccurately described by RPA. The approximate exchange kernel (AXK), which is a beyond-RPA correction results in a much more accurate description of the PEC around the equilibrium bond distance for molecular radicals since it partially corrects the self-correlation error of RPA. [42]

1.3 Conclusions

The analytical gradients within the post-KS RPA using the RI approximation (RIRPA) was successfully extended for open-shell systems. The accuracy of this implementation was tested for a set of molecules and MAE for RPA based on TPSS and PBE SL inputs were found to be 0.51 pm and 0.56 pm, respectively. Thus RPA is a reliable method for calculations of first-order properties of not just closed-shell systems but also radicals with open-shell electronic structure.

Chapter 2

Generalized Kohn-Sham semicanonical projected RPA

 This material is based upon work supported by the National Science Foundation under CHE−1464828 and CHE−1800431.

2.1 Introduction and Summary

Electronic structure methods based on the random-phase approximation (RPA) [21, 22] are rapidly gaining popularity in solid-state and molecular applications [32, 33, 63]. As opposed to semilocal (SL) density functional approximations (DFAs), RPA-based methods capture noncovalent interactions [64], which have recently moved into the focus of research in soft matter, nanomaterials, and catalysis [65]. RPA-based methods are comparable in cost with but more robust than perturbative approaches for small-gap systems and offer a way out of the functional inflation dilemma faced by SL DFAs [34].

The vast majority of today's RPA calculations are performed in a "post Kohn–Sham" fashion, i.e., by evaluating the RPA energy functional using Kohn–Sham (KS) orbitals generated from a variational SL DFA calculation [31]. Apart from the lack of a variationally stable energy, a major limitation of this SL-RPA approach is that SL densities are relatively inaccurate for open-shell systems, negative ions, and small-gap compounds, producing large "density-driven errors" in energies and other properties [66, 67]. For example, SL DFAs produce qualitatively incorrect densities and ionization potentials for negative ions [16], and overly delocalized states for correlated materials [68].

Unlike SL energy functionals, the RPA energy explicitly depends on the unknown KS potential, making straightforward minimization with respect to the density or KS orbitals impossible. In this paper, we distinguish density- or orbital-selfconsistent (OSC) RPA approaches, which minimize the energy after choosing an approximate KS potential, from functional selfconsistent (FSC) approaches, which aim to determine the KS potential functional self-consistently by requiring its exchange-correlation (XC) part to coincide with the functional derivative of the RPA energy. The optimized effective potential (OEP) approach [69–72] has been claimed to achieve "fully selfconsistent" RPA results [71]. However, while OEP-RPA produces accurate KS orbital energies, OEP-RPA results for bond energies and noncovalent

interactions are less accurate than their SL-RPA counterparts [71]. This result is puzzling, because the OEP-RPA KS potentials are considerably more accurate than SL ones [73], and recent orbital-optimized RPA approaches improve upon SL RPA energetics [74].

Observables such as quasiparticle spectra and ionization potentials (IPs) have traditionally been the domain of many-body Green's function theory (GFT) [75–77]. For example, quasiparticle self-consistent *GW* theory [78, 79] yields highly accurate IPs and band gaps for a wide variety of materials, but accurate total energy differences and related properties such as structures or thermodynamic quantities remain elusive. *GW* approaches starting from SL DFAs [80–82] and even fully self-consistent *GW* [83] face a similar dilemma, producing high quality quasiparticle spectra and excitation energies, but energy differences generally inferior to SL-RPA [84, 85].

Here we generalize the SL-RPA energy functional using a simple semicanonical projection (sp) of the SL KS Hamiltonian. The resulting spRPA energy is a functional of the KS one-particle density matrix that may variationally be minimized using an OSC generalized KS (GKS) scheme [86]. Semicanonical approaches have successfully been used to devise perturbative corrections to SL-RPA in the past [87]. The present variational GKS spRPA method is designed to (i) recover SL-RPA for SL densities; (ii) reduce density-driven error by determining the density from the stationary point of the RPA rather than a SL energy functional; (iii) systematically improve SL-RPA energetics; (iv) approximate FSC RPA without sacrificing the variational principle; (v) yield a complete GKS effective one-particle Hamiltonian, unlike orbital optimized [74] or Brueckner [88] RPA, providing an intuitive one-electron picture and GKS orbital energies which accurately approximate quasiparticle spectra [89]; (vi) establish a straightforward connection to GFT and *GW* theory; (vii) eliminate the need for KS inversion or OEP approaches, which can be ill conditioned [90] and require cumbersome regularization [91–93].

2.2 Variational Minimization of Potential-Dependent Functionals

2.2.1 Statement of the Problem

Variational minimization of a functional with respect to the density or the KS orbitals requires knowledge at least of the energy functional and its functional derivative for a given trial density. Here we consider functionals that depend on the density $\rho(x)$ through the KS orbitals and occupation numbers $|\phi_p\rangle$ and n_p *and explicitly* on the KS potential $\mathrm{V}_s[\rho](x)$; $x = (\mathbf{r}, \sigma)$ denotes space-spin coordinates. This large class includes functionals derived from many-body perturbation theory [94–96] as well as RPA. The resulting XC energy thus takes the general form

$$E^{\mathrm{XC}}[\rho] = E^{\mathrm{XC}}[|\boldsymbol{\phi}[\rho]\rangle, \mathbf{n}[\rho], \mathrm{V}_s[\rho]], \tag{2.1}$$

where the KS orbitals and occupation numbers were gathered in the column vectors $|\boldsymbol{\phi}\rangle, \mathbf{n}$.

Kohn and Sham[5] showed that variational minimization of the total energy as a functional of ρ leads to the KS equations

$$\mathrm{H}_0[\rho]\,|\phi_p\rangle = \epsilon_p\,|\phi_p\rangle\,, \tag{2.2}$$

where $\mathrm{H}_0[\rho] = \mathrm{T} + \mathrm{V}_s[\rho]$ is the noninteracting KS one-particle Hamiltonian, T is the one-particle kinetic energy operator, and

$$\mathrm{V}_s[\rho](x) = \mathrm{V}^{\mathrm{ext}}(x) + \mathrm{V}^{\mathrm{H}}[\rho](x) + \mathrm{V}^{\mathrm{XC}}[\rho](x) \tag{2.3}$$

is the KS one-particle potential. $\mathrm{V}^{\mathrm{ext}}(x)$ is the external one-particle potential, and $\mathrm{V}^{\mathrm{H}}[\rho](x)$

is the Hartree potential. The XC potential is the (total) functional derivative of the XC energy with respect to the density,

$$\mathrm{V}^{\mathrm{XC}}[\rho](x) = \frac{\delta E^{\mathrm{XC}}[\rho]}{\delta \rho(x)}. \tag{2.4}$$

The OSC minimizing density is given by

$$\rho(x) = \sum_p n_p |\phi_p(x)|^2, \tag{2.5}$$

with occupation numbers normally [97] chosen according to the Aufbau principle. While this section focuses on density-based "proper KS" schemes, analogous considerations apply to the GKS framework [86], if the local XC potential in Eq. (2.4) is replaced by the nonlocal one defined by the functional derivative of the XC energy with respect to the KS density matrix.

However, Eqs. (2.1)-(2.5) do not completely determine the energy as a functional of the density: Obtaining the KS potential via Eq. (2.4) requires knowledge of $E^{\mathrm{XC}}[\rho]$, which in turn is defined in terms of the KS potential. Two different avenues have been used to bypass this quandary: The first uses the density (or, in GKS framework, the orbitals and occupation numbers) as independent variable. In this case, an additional condition specifying the KS potential as a functional of the density (or the orbitals and occupation numbers) is required. The second approach considers the density (or the orbitals and occupation numbers) as dependent variable(s), and the potential as independent variable. This potential-functional approach requires specification of the density (or the orbitals and occupation numbers) as functional of the potential. In the following, we discuss different choices for either functional(s), which lead to qualitatively different XC energy functionals, labeled by subscripts *a*-*d*.

2.2.2 KS Potentials and Energy Functionals

Semilocal Potentials. Since SL KS potentials are readily available, a straightforward choice for the XC energy functional is

$$E_a^{\mathrm{XC}}[\rho] = E^{\mathrm{XC}}[|\boldsymbol{\phi}[\rho]\rangle\,, \mathbf{n}[\rho], \mathrm{V}_s^{\mathrm{SL}}[\rho]]. \tag{2.6}$$

Here, the SL XC potential is the functional derivative of a SL XC energy functional such as PBE [7],

$$\mathrm{V}^{\mathrm{XC\ SL}}[\rho](x) = \frac{\delta E^{\mathrm{XC\ SL}}[\rho]}{\delta\rho(x)}, \tag{2.7}$$

and $\mathrm{V}_s^{\mathrm{SL}}[\rho]$ is obtained by replacing $\mathrm{V}^{\mathrm{XC}}[\rho]$ with $\mathrm{V}^{\mathrm{XC\ SL}}[\rho]$ in Eq. (2.3).

The main drawback of this approach is that it violates Eq. (2.4),

$$\frac{\delta E_a^{\mathrm{XC}}[\rho]}{\delta\rho(x)} \neq \mathrm{V}^{\mathrm{XC\ SL}}[\rho](x). \tag{2.8}$$

As a result, there are two KS systems, one related to minimization of $E_a^{\mathrm{XC}}[\rho]$, and the other generated by $\mathrm{V}^{\mathrm{XC\ SL}}[\rho]$, whose density is generally different from the orbital density ρ. The XC energy is defined in terms of the relatively inaccurate SL potential, giving rise to density-driven error. In explorative calculations using the RPA energy functional, the total energy differences we obtained from such schemes were not significantly more accurate than the post-KS semilocal ones.

"Exact" Potentials Via KS Inversion or OEP. For a noninteracting v-representable trial density, the "exact" KS potential $\mathrm{V}_s[\rho]$ (and thus $\mathrm{H}_0[\rho]$) may be determined, up to a constant, by inversion of the KS equations. One thus might wonder if this choice results in better properties than the use of SL potentials. While the uniqueness of $\mathrm{V}_s[\rho]$ is guaranteed

by the Hohenberg–Kohn theorem [3], general trial densities may not be pure-state noninteracting v-representable; see, e.g., Ref. [98] for examples. In common finite basis sets, this condition is rarely satisfied [99], and KS inversion procedures can be ill-posed [100].

The OEP approach claims to bypass some of these difficulties [69–71, 95] by using the local KS potential $\mathrm{V}_s(x)$ as independent variable[101, 102] and the KS orbitals $\phi_p[\mathrm{V}_s]$ and occupation numbers $n_p[\mathrm{V}_s]$ as dependent variables; the functionals $\phi_p[\mathrm{V}_s]$ and $n_p[\mathrm{V}_s]$ are defined by the requirement that they satisfy the KS equations (2.2) and minimize the total KS kinetic energy. The resulting XC energy thus becomes a potential functional,

$$E_b^{\mathrm{XC}}[\mathrm{V}_s] = E_b^{\mathrm{XC}}[|\boldsymbol{\phi}[\mathrm{V}_s]\rangle\,, \mathbf{n}[\mathrm{V}_s], \mathrm{V}_s]. \tag{2.9}$$

To make a connection to density functionals, OEP methods consider the density generated by the KS orbitals and occupation numbers,

$$\rho_s[\mathrm{V}_s](x) = \sum_p n_p[\mathrm{V}_s]|\phi_p[\mathrm{V}_s](x)|^2. \tag{2.10}$$

By the HK theorem, V_s is a functional of ρ_s, and thus the XC potential can be obtained from the chain rule,

$$\frac{\delta E_b^{\mathrm{XC}}[\mathrm{V}_s]}{\delta \mathrm{V}_s(x)} = \int dx' \frac{\delta E_b^{\mathrm{XC}}[\rho_s]}{\delta \rho_s(x')} \frac{\delta \rho_s[\mathrm{V}_s](x')}{\delta \mathrm{V}_s(x)}. \tag{2.11}$$

Since $\rho_s[\mathrm{V}_s]$ is the KS density, $\delta\rho_s[\mathrm{V}_s](x')/\delta\mathrm{V}_s(x)$ is the well-known KS density-density response function, which is an explicit functional of the KS orbitals and orbital energies for a given potential V_s [71, 95], and Eq. (2.11) becomes the OEP integral equation [103]. While grid-based OEP approaches are fairly straightforward, basis-set OEP approaches can be ill-posed similar to KS inversion [90] and require additional regularization [91–93].

OEP approaches to potential-dependent XC functionals have been dubbed "fully selfcon-

sistent" [71, 104]. Even though they use the "exact" KS potential, however, they lack functional selfconsistency, causing the KS density ρ_s to differ from the functional derivative of the energy with respect to the external potential:

In potential functional theory, the density as a functional of the KS potential is *defined* by

$$\frac{\delta E[\mathrm{V}_s]}{\delta \mathrm{V}^{\mathrm{ext}}(x)} = \rho[\mathrm{V}_s](x), \tag{2.12}$$

where $E[\mathrm{V}_s]$ is the total energy potential functional [101, 105]. Eq. (2.12) is the equivalent of Eq. (2.4) in density functional theory and thus fundamental; it may be viewed a consequence of the Hellmann-Feynman theorem, and as such is commonly used to define the density and all related properties even for approximate energy functionals. For inexact XC functionals with explicit dependence on the KS potential, however, the KS density, defined by Eq. (2.10), generally differs from the exact one, defined by Eq. (2.12): Evaluating the functional derivative of the total energy expression defined by the potential functional $E_b^{\mathrm{XC}}[\mathrm{V}_s]$ in Eq. (2.9) using the Hellmann-Feynman theorem and Eq. (2.12) yields

$$\rho_s[\mathrm{V}_s] + \left(\frac{\delta E_b^{\mathrm{XC}}[\mathrm{V}_s]}{\delta \mathrm{V}_s(x)}\right)_{|\boldsymbol{\phi}[\mathrm{V}_s]\rangle,\mathbf{n}[\mathrm{V}_s]} = \rho_b[\mathrm{V}_s](x), \tag{2.13}$$

where the functional derivative is a partial derivative at fixed orbitals and occupation numbers, and $\rho_b[\mathrm{V}_s](x) = \delta E_b[\mathrm{V}_s]/\delta \mathrm{V}^{\mathrm{ext}}(x)$ is the Hellmann-Feynman density generated by $E_b^{\mathrm{XC}}[\mathrm{V}_s]$. The quantity

$$\rho_b^{\mathrm{XC}}[\mathrm{V}_s](x) = \left(\frac{\delta E_b^{\mathrm{XC}}[\mathrm{V}_s]}{\delta \mathrm{V}_s(x)}\right)_{|\boldsymbol{\phi}[\mathrm{V}_s]\rangle,\mathbf{n}[\mathrm{V}_s]}, \tag{2.14}$$

is zero for the exact XC functional by construction, but generally nonzero for the approximate explicitly potential-dependent XC functionals discussed here (see, e.g., Ref. [71] and Sec.

2.3.2 for examples). An immediate consequence is that

$$\frac{\delta E_b^{\mathrm{XC}}[\rho_s]}{\delta \rho_s(x)} \neq \frac{\delta E_b^{\mathrm{XC}}[\rho_b]}{\delta \rho_b(x)}, \tag{2.15}$$

i.e., the OEP XC potential produces the functional derivative of the XC energy with respect to the noninteracting KS density ρ_s rather than $\rho_b[\mathrm{V}_s]$, which is the correct density by Eq. (2.12).

In conclusion, even using the "exact" KS potential produces the paradoxical result of two different densities corresponding to two different KS potentials, and the less accurate of the two (according to the Hellmann-Feynman theorem) is used to obtain the total energy. This confirms that lacking functional selfconsistency is a fundamental problem of explicitly potential-dependent functionals which, contrary to previous suggestions [71, 95], cannot be remedied by the OEP approach.

Functional-Selfconsistent Potentials. The paradoxical result of two different densities and KS potentials are caused by inconsistency of the KS potentials defining the XC energy functional with the functional derivative thereof. A resolution is possible if the KS potential satisfies the functional selfconsistency condition

$$\rho^{\mathrm{XC}}[|\boldsymbol{\phi}\rangle, \mathbf{n}, \mathrm{V}_s](x) = 0. \tag{2.16}$$

By Eq. (2.13), the orbitals and occupation numbers generated by such an FSC KS potential yield the correct Hellmann-Feynman density, and thus Eq. (2.16) is an exact constraint for the KS potential V_s. Eq. (2.16) is equivalent to requiring the XC energy functional to be stable with respect to variations of the KS potential at fixed orbitals and occupation

numbers. Thus, the chain rule yields for the FSC XC potential

$$\begin{aligned} \mathrm{V}^{\mathrm{XC}}[|\boldsymbol{\phi}\rangle, \mathbf{n}, \mathrm{V}_s](x) &= \frac{\delta E^{\mathrm{XC}}[|\boldsymbol{\phi}\rangle, \mathbf{n}, \mathrm{V}_s]}{\delta \rho(x)} \\ &= \left(\frac{\delta E^{\mathrm{XC}}[|\boldsymbol{\phi}\rangle, \mathbf{n}, \mathrm{V}_s]}{\delta \rho(x)} \right)_{\mathrm{V}_s}, \end{aligned} \tag{2.17}$$

since the partial derivative with respect to V_s vanishes according to Eq. (2.16). For potential-independent XC functionals, the partial derivative is a total derivative, and Eq. (2.17) reduces to the conventional definition of the XC potential. For potential-dependent XC functionals, Eq. (2.17) is a statement of the functional selfconsistency condition.

It may be possible to define a FSC XC potential $\mathrm{V}_{s,c}[|\boldsymbol{\phi}\rangle, \mathbf{n}]$ as a functional of the orbitals and occupation numbers implicitly by Eqs. (2.16) or (2.17). The conditions under which the functional selfconsistency constraint uniquely determines $\mathrm{V}_{s,c}$ and the resulting XC energy functional

$$E_c^{\mathrm{XC}}[|\boldsymbol{\phi}\rangle, \mathbf{n}] = E^{\mathrm{XC}}[|\boldsymbol{\phi}\rangle, \mathbf{n}, \mathrm{V}_{s,c}[|\boldsymbol{\phi}\rangle, \mathbf{n}]] \tag{2.18}$$

depend on the specific form of the XC energy functional (2.1). If such a unique potential $\mathrm{V}_{s,c}$ exists, then the density (or KS orbitals and occupation numbers) minimizing the energy functional associated with E_c^{XC} are generated by it, because, by Eq. (2.17), $\mathrm{V}_{s,c}$ is obtained from the functional derivative of E_c^{XC}. At the same time, Eq. (2.16) guarantees that the resulting KS density equals the Hellman-Feynman one. In this sense, the FSC KS potential is optimal for a given explicitly potential-dependent energy functional.

It is important to distinguish orbital and functional selfconsistency in such a scheme: The latter determines the KS potential and thus the energy functional for *fixed* density, while the former determines the minimizing density (or the KS orbitals and occupation numbers). Mixing the two may produce ill-defined energy functionals, causing problems such as initial state dependence and multiple solutions familiar from selfconsistent GFT approaches [106].

Semicanonical KS. The above analysis suggests that lack of functional selfconsistency of SL and OEP KS potentials critically limits the accuracy of these approaches. We take a step towards a fully FSC solution by constructing an approximation to the FSC KS Hamiltonian, which leads to an explicit energy functional of the orbitals and occupation numbers. Using a GKS framework to achieve orbital selfconsistency allows us to bypass the numerical challenges of OEP methods and obtain orbital energies corresponding to physical ionization potentials and electron affinities.

Rather than imposing the full functional selfconsistency condition, which implies that the KS potential entering the XC energy functional is identical to the functional derivative thereof, see Eq. (2.17), we only require that the KS potential defining the XC energy generate the same eigenstates (up to unitary equivalence) as the one obtained from functional differentiation. This weaker condition is readily imposed by semicanonical projection of a readily available SL KS Hamiltonian $\mathrm{H}_0^{\mathrm{SL}}$. In the most general case, the KS density matrix takes the form

$$\mathrm{D} = \sum_{\lambda\lambda'} \mathrm{P}_\lambda \mathrm{n}_{\lambda\lambda'} \mathrm{P}_{\lambda'}, \tag{2.19}$$

where P_λ denotes orthogonal projectors belonging to blocks of KS orbitals with degenerate occupation numbers, and $\mathrm{n}_{\lambda\lambda'} = \mathrm{n}_\lambda \delta_{\lambda\lambda'}$ is diagonal, with n_λ denoting occupation number matrices [107]. For example, for integer KS occupations $1, 0$, there are two distinct matrices n_λ with eigenvalues $n_\lambda = 1, 0$. The sp KS Hamiltonian is defined by

$$\tilde{\mathrm{H}}_0 = \sum_{\lambda} \mathrm{P}_\lambda \mathrm{H}_0^{\mathrm{SL}} \mathrm{P}_\lambda, \tag{2.20}$$

and contains only the diagonal ($\lambda = \lambda'$) blocks of $\mathrm{H}_0^{\mathrm{SL}}$. $\tilde{\mathrm{H}}_0$ commutes with D by construction; thus, one may find a common "semicanonical" basis in which both $\tilde{\mathrm{H}}_0$ and a given KS density matrix are diagonal. Moreover, $\tilde{\mathrm{H}}_0$ is invariant under unitary transformations of KS orbitals

with degenerate occupation numbers, since the projectors P_λ are invariant. If D is generated by $\mathrm{H}_0^{\mathrm{SL}}$, then $\tilde{\mathrm{H}}_0 = \mathrm{H}_0^{\mathrm{SL}}$; perturbation theory implies that the deviation of the sp orbital energies from the SL ones is quadratic in $\mathrm{H}_0^{\mathrm{SL}} - \tilde{\mathrm{H}}_0$. The nonlocal sp XC potential may thus be defined as

$$\tilde{\mathrm{V}}^{\mathrm{XC}}[|\boldsymbol{\phi}\rangle, \mathbf{n}] = \mathrm{V}^{\mathrm{XC\ SL}}[\rho] + \tilde{\mathrm{H}}_0[|\boldsymbol{\phi}\rangle, \mathbf{n}] - \mathrm{H}_0^{\mathrm{SL}}[\rho], \tag{2.21}$$

and the corresponding sp XC energy functional,

$$E_d^{\mathrm{XC}}[|\boldsymbol{\phi}\rangle, \mathbf{n}] = E^{\mathrm{XC}}[|\boldsymbol{\phi}\rangle, \mathbf{n}, \tilde{\mathrm{V}}^{\mathrm{XC}}[[|\boldsymbol{\phi}\rangle, \mathbf{n}]], \tag{2.22}$$

is an explicit functional of the KS orbitals and occupation numbers only, which may be subject to OSC optimization using GKS methodology. We will thus focus on functional of type $E_d^{\mathrm{XC}}[|\boldsymbol{\phi}\rangle, \mathbf{n}]$ in the following.

2.2.3 spRPA Energy Functional

For a given KS determinant Φ, the RPA total energy,

$$E^{\mathrm{RPA}} = \langle\Phi|\mathrm{H}|\Phi\rangle + E^{\mathrm{C\ RPA}}, \tag{2.23}$$

equals the expectation value of the physical Hamiltonian H plus the RPA correlation energy, [29, 108]

$$E^{\mathrm{C\ RPA}} = -\frac{1}{2}\int_0^1 d\alpha \Im \int_{-\infty}^{\infty} \frac{d\omega}{2\pi} \langle \left(\Pi_\alpha^{\mathrm{RPA}}(\omega) - \Pi_0(\omega)\right) \mathrm{V}\rangle. \tag{2.24}$$

V is the bare electron-electron Coulomb interaction, $\Pi_\alpha^{\mathrm{RPA}}(\omega) = (1 - \alpha\Pi_0(\omega)\mathrm{V})^{-1}\Pi_0(\omega)$ denotes the time-ordered RPA polarization propagator at coupling strength α and real fre-

quency ω, and $\Pi_0(\omega)$ is its noninteracting KS equivalent; brackets stand for traces. The rank four operator $\Pi_0(\omega)$ factorizes as [109]

$$\Pi_0(\omega) = \int_{-\infty}^{\infty} \frac{d\omega'}{2\pi i} \mathrm{G}_0(\omega') \otimes \mathrm{G}_0(\omega' - \omega), \tag{2.25}$$

into a convolution product of one-particle KS Green's functions $\mathrm{G}_0(\omega)$.

The KS Green's function corresponding to the sp KS Hamiltonian $\tilde{\mathrm{H}}_0$ is

$$\mathrm{G}_0(\omega) = \mathrm{n}^{1/2}(\omega - \tilde{\mathrm{H}}_0 - i0^+)^{-1}\mathrm{n}^{1/2} + (1-\mathrm{n})^{1/2}(\omega - \tilde{\mathrm{H}}_0 + i0^+)^{-1}(1-\mathrm{n})^{1/2}; \tag{2.26}$$

this symmetrized form remains Hermitian even for density matrix variations causing off-diagonal occupation number matrices. By construction, $\mathrm{G}_0(\omega)$ reproduces D,

$$\mathrm{D} = \int_{-\infty}^{\infty} \frac{d\omega}{2\pi i} e^{i\omega 0^+} \mathrm{G}_0(\omega). \tag{2.27}$$

On the other hand, the quasiparticle spectrum of the sp Green's function is given by the semicanonical KS eigenvalues of $\tilde{\mathrm{H}}_0$, which approximate the semilocal ones in a perturbative sense.

Eqs. (2.20)-(2.26) define the spRPA energy as a functional of the KS density matrix, $E^{\mathrm{spRPA}}[\mathrm{D}]$, or, equivalently, the spectral projectors P_λ and occupation number matrices n_λ – clearly, a functional of type *d* according to Sec. 2.2.2. $E^{\mathrm{spRPA}}[\mathrm{D}]$ depends on the SL XC potential DFA entering $\tilde{\mathrm{H}}_0$, for which we choose PBE [7]. This introduces a dependence on the choice of SL potential; however, this dependence is less strong than for SL-RPA, since the current scheme is OSC and partially FSC, and even for SL-RPA, the dependence of energy difference on the specific choice of SL potential is moderate [63]. The spRPA energy functional is conveniently evaluated by expressing G_0 in the semicanonical basis, factorizing the interaction V, and performing the frequency integration along the imaginary axis, in

analogy to SL-RPA [35].

2.3 Variational GKS Minimization of Semicanonical Projected RPA

2.3.1 Energy Lagrangian and Euler Equations

Within the GKS-spRPA formalism, the ground state energy is obtained as the minimum of the spRPA energy functional with respect to D, subject to the Fermion N-representability constraint that D have eigenvalues between 0 and 1 whose sum is the total electron number N. We explicitly impose the latter by the substitution $\mathrm{n} = \mathrm{m}^\dagger\mathrm{m}$, where the Hermitian matrices m satisfy $\langle \mathrm{m}^\dagger\mathrm{m}\rangle = N$. The GKS-spRPA energy Lagrangian is thus

$$L^{\mathrm{spRPA}}[|\boldsymbol{\phi}\rangle, \mathrm{m}, \eta, \mu] = E^{\mathrm{spRPA}}[\mathrm{D}[|\boldsymbol{\phi}\rangle, \mathrm{m}]] - \langle \eta(\langle\boldsymbol{\phi}|\boldsymbol{\phi}\rangle - 1)\rangle - \mu\left(\langle \mathrm{m}^\dagger\mathrm{m}\rangle - N\right). \quad (2.28)$$

Here, the GKS orbitals were gathered in the transpose vectors $|\boldsymbol{\phi}\rangle$, i.e., $\langle\boldsymbol{\phi}|\boldsymbol{\phi}\rangle$ is a matrix with respect to GKS orbital indices (but a scalar with respect to the one-particle Hilbert space). In this notation, the GKS density matrix becomes

$$\mathrm{D}[|\boldsymbol{\phi}\rangle, \mathrm{m}] = |\boldsymbol{\phi}\rangle\, \mathrm{m}^\dagger\mathrm{m}\, \langle\boldsymbol{\phi}|\,. \quad (2.29)$$

the Hermitian Lagrange multiplier matrix η enforces orbital orthonormality, and the real scalar Lagrange multiplier μ accounts for normalization of D. The present approach is a special case of variational density matrix functional minimization [107, 110, 111]. A necessary condition for a minimum of the GKS-spRPA energy subject to the above constraints is that

the first partial derivatives of L^{spRPA} with respect to all variational parameters vanish.

Requiring stationarity with respect to the GKS orbitals leads to the GKS self-consistent field (SCF) equations

$$\mathrm{H}_0^{\mathrm{spRPA}}[\mathrm{D}]\,\mathrm{n}\,|\boldsymbol{\phi}\rangle = \eta\,|\boldsymbol{\phi}\rangle\,, \tag{2.30}$$

where the effective one-particle GKS-spRPA Hamiltonian is defined as the functional derivative of the spRPA energy with respect to the GKS density matrix,

$$\mathrm{H}_0^{\mathrm{spRPA}}[\mathrm{D}] = \frac{\delta E^{\mathrm{spRPA}}[\mathrm{D}]}{\delta \mathrm{D}}. \tag{2.31}$$

Eq. (2.30) is equivalent to

$$\mathrm{H}_0^{\mathrm{spRPA}}\mathrm{n} = \eta. \tag{2.32}$$

The Hermiticity of all three matrices in the previous equation then implies that $\mathrm{H}_0^{\mathrm{spRPA}}$ and n commute, and since n is block-diagonal, so must be $\mathrm{H}_0^{\mathrm{spRPA}}$, i.e., matrix elements of the spRPA Hamiltonian between orbitals belonging to different occupation number blocks must vanish ("Brillouin's Theorem"). Evaluating n_λ as $\mathrm{n}_{ij\lambda} = n_\lambda \delta_{ij}$, where indices i, j label orbitals with identical occupation numbers n_λ, and defining the Hermitian matrices

$$\epsilon_{\lambda\lambda'} = \begin{cases} 0 & \lambda \neq \lambda', \\ \eta_{\lambda\lambda}/n_\lambda & \lambda = \lambda', \end{cases} \tag{2.33}$$

Eq. (2.30) takes a more familiar form,

$$\mathrm{H}_0^{\mathrm{spRPA}}[\mathrm{D}]\,|\phi_{i\lambda}\rangle = \sum_j \epsilon_{ij\lambda}\,|\phi_{j\lambda}\rangle\,. \tag{2.34}$$

Eq. (2.34) is form-invariant under unitary transformations of orbitals belonging to degenerate

occupation numbers n_λ. A unique "canonical" GKS-spRPA orbital basis may be defined by requiring $\epsilon_{ij\lambda}$ to be diagonal with elements $\epsilon_{i\lambda}$, in which case takes the form of the canonical GKS equations,

$$\mathrm{H}_0^{\mathrm{spRPA}}[\mathrm{D}]\,|\phi_{i\lambda}\rangle = \epsilon_{i\lambda}\,|\phi_{i\lambda}\rangle\,, \tag{2.35}$$

which need to be solved iteratively along with the orthonormality and normalization constraints.

The occupation numbers are determined by the stationarity condition for m,

$$(\mathrm{H}_0^{\mathrm{spRPA}} - \mu)\mathrm{m} = 0. \tag{2.36}$$

In the canonical basis, Eq. (2.36) simplifies to $(\epsilon_{i\lambda} - \mu)n_\lambda^{1/2} = 0$. The second variation of L^{spRPA} with respect to m is nonnegative for bound states with an Aufbau occupation, i.e., for all i,

$$n_\lambda = \begin{cases} 1; & \epsilon_{i\lambda} < \mu \\ 0; & \epsilon_{i\lambda} > \mu \end{cases}, \tag{2.37}$$

where the ionization potential μ is chosen such that the normalization condition $\langle \mathrm{n} \rangle = N$ is satisfied. If $\epsilon_{i\lambda} = \mu$, then any n_λ with $0 \leq n_\lambda \leq 1$ yielding correct normalization is permissible[107].

2.3.2 One-Particle GKS-spRPA Hamiltonian

The effective one-particle GKS-spRPA Hamiltonian may be analyzed by decomposing the functional derivative in Eq. (2.31) according to

$$\mathrm{H}_0^{\mathrm{spRPA}}[\mathrm{D}] = \mathrm{H}_0^{\mathrm{HF}}[\mathrm{D}] + \mathrm{V}^{\mathrm{C\ spRPA}}[\mathrm{D}]. \tag{2.38}$$

Here, $\mathrm{H}_0^{\mathrm{HF}}[\mathrm{D}]$ is the well-known Hartree-Fock one-particle Hamiltonian, and $\mathrm{V}^{\mathrm{C\ spRPA}}[\mathrm{D}]$ denotes the nonlocal RPA correlation potential resulting from the functional derivative of the spRPA correlation energy. Since the spRPA correlation energy depends on D only through the sp Green's function, Eq. (2.26), the functional chain rule yields

$$\mathrm{V}^{\mathrm{C\ spRPA}}[\mathrm{D}] = \int_{-\infty}^{\infty} \frac{d\omega}{2\pi} \Sigma^{\mathrm{C}}(\omega) \frac{\delta \mathrm{G}_0(\omega)}{\delta \mathrm{D}}. \tag{2.39}$$

The functional derivative $\delta \mathrm{G}_0(\omega)/\delta \mathrm{D}$ is a rank-four tensor operator.

$$\Sigma^{\mathrm{C}}(\omega) = \frac{\delta E^{\mathrm{C\ spRPA}}}{\delta \mathrm{G}_0(\omega)} \tag{2.40}$$

is the correlation part of the RPA self-energy [73]. Eqs. (2.39) and (2.40) hold for any correlation energy functional of the GKS Green's function, and reveal the close connection of the GKS correlation potential and the corresponding self-energy. If the correlation energy further depends on G_0 through Π_0 only, then the functional chain rule may be used once more to show that the correlation self-energy has the form[75, 76]

$$\Sigma^{\mathrm{C}}(\omega) = \int_{-\infty}^{\infty} \frac{d\omega'}{\pi i} \mathrm{W}^{\mathrm{C}}(\omega') \mathrm{G}_0(\omega' - \omega). \tag{2.41}$$

The correlation part of the effective interaction

$$\mathrm{W}^{\mathrm{C}}(\omega) = \frac{\delta E^{\mathrm{C\ RPA}}}{\delta \Pi_0(\omega)} \tag{2.42}$$

is also a rank four tensor operator. Within RPA,

$$\mathrm{W}^{\mathrm{C}}(\omega) = \mathrm{V}(1 - \Pi_0(\omega)\mathrm{V})^{-1}; \tag{2.43}$$

thus, $\Sigma^{\mathrm{C}}(\omega)$ is identical to the correlation part of the *GW* self-energy [112, 113], evaluated at the spGKS Green's function.

To gain further insight into the physical meaning of the nonlocal RPA correlation potential, one may decompose the total density matrix derivative into a sum of three partial derivatives,

$$\mathrm{V}^{\mathrm{C\ spRPA}}[\mathrm{D}] = \mathrm{V}^{\mathrm{C},1}[\mathrm{D}] + \mathrm{V}^{\mathrm{C},2}[\mathrm{D}] + \mathrm{V}^{\mathrm{C},3}[\mathrm{D}]. \tag{2.44}$$

The first term corresponds to the partial density matrix derivative at fixed sp Hamiltonian $\tilde{\mathrm{H}}_0$. Denoting (anti)commutators by (curly) brackets, this part of the potential is found to be

$$\mathrm{V}^{\mathrm{C},1}_{\lambda\lambda'} = \int \frac{d\omega}{2\pi} \begin{cases} \frac{1}{n_\lambda - n_{\lambda'}} \left[\mathrm{G}_0(\omega), \Sigma^{\mathrm{C}}(\omega)\right]_{\lambda\lambda'}, & \lambda \neq \lambda', \\ \pi i \left\{\delta(\omega - \tilde{\mathrm{H}}_0), \Sigma^{\mathrm{C}}(\omega)\right\}_{\lambda\lambda'}, & \lambda = \lambda'. \end{cases} \tag{2.45}$$

The off-diagonal ($\lambda \neq \lambda'$) blocks of $\mathrm{V}^{\mathrm{C},1}$ reduce to the gradient of the RPA energy with respect to orbital rotations, thus establishing a link to orbital-optimized RPA approaches [74]. The diagonal ($\lambda = \lambda'$) blocks, on the other hand, result from variations corresponding to changes in the occupation numbers and cannot be obtained in an orbital optimization framework. In the semicanonical basis, the λ blocks of $\tilde{\mathrm{H}}_0$ are diagonal,

$$\tilde{\mathrm{H}}_{0ij\lambda} = \delta_{ij}\tilde{\epsilon}_{i\lambda}, \tag{2.46}$$

and thus the diagonal blocks of $\mathrm{V}^{\mathrm{C},1\ \mathrm{spRPA}}$ take the form

$$\mathrm{V}^{\mathrm{C},1}_{ij\lambda} = \frac{i}{2}\left(\Sigma^{\mathrm{C}}_{\lambda ij}(\tilde{\epsilon}_{i\lambda}) + \Sigma^{\mathrm{C}}_{\lambda ji}(\tilde{\epsilon}_{j\lambda})\right). \tag{2.47}$$

Perturbative expansion of the GKS-spRPA orbital energies around the SL ground state solution reveals the physical significance of Eq. (2.47):

$$\epsilon_{i\lambda} = \epsilon^{\mathrm{SL}}_{i\lambda} + i\Sigma^{\mathrm{XC}}_{ii\lambda}(\epsilon^{\mathrm{SL}}_{i\lambda}) + V^{\mathrm{C},3}_{ii\lambda} - V^{\mathrm{XC\ SL}}_{ii\lambda} + O(\|\mathrm{H}_0^{\mathrm{spRPA}} - \mathrm{H}_0^{\mathrm{SL}}\|^2). \tag{2.48}$$

Here, $\Sigma^{\mathrm{XC}}(\omega)$ is the XC self-energy within the G_0W_0 approximation, and $V^{\mathrm{XC\ SL}}$ is the SL XC potential. The GKS-spRPA orbital energies hence reduce to the quasiparticle GW energies with unit normalization factor [76] in a perturbative first-order SCF sense apart from $\mathrm{V}^{\mathrm{C},3}$, which is typically small compared to $\mathrm{V}^{\mathrm{C},1}$.

The remaining parts of the GKS-spRPA correlation potential arise from changes in $\tilde{\mathrm{H}}_0$. The second term accounts for the semicanonical projection and its diagonal part vanishes,

$$\mathrm{V}^{\mathrm{C},2}_{\lambda\lambda'} = \begin{cases} \frac{1}{n_\lambda - n_{\lambda'}}[\mathrm{H}_0^{\mathrm{SL}}, \mathrm{T}]_{\lambda\lambda'}, & \lambda \neq \lambda', \\ 0, & \lambda = \lambda', \end{cases} \tag{2.49}$$

Here, the RPA unrelaxed difference density matrix [43] or first-order density matrix [113]

$$\mathrm{T} = \frac{\delta E^{\mathrm{C\ spRPA}}}{\delta \tilde{\mathrm{H}}_0} \tag{2.50}$$

familiar from RPA analytical derivative theory has been introduced. Since the spGKS RPA Lagrangian is stationary at the converged spGKS density matrix D, there are no additional "orbital relaxation" terms, and the corresponding total interacting spRPA one-particle density matrix is simply $\mathrm{D} + \mathrm{T}$; an explicit expression for T is provided in Appendix A.1. The

density generated by T equals $\rho^{\mathrm{XC}}(x)$, Eq. (2.14). Since GKS-spRPA is not fully FSC, $\rho^{\mathrm{XC}}(x)$ does not vanish, but is found to be small in most circumstances. The remaining part of the correlation potential,

$$\mathrm{V}^{\mathrm{C},3} = \mathrm{F}^{\mathrm{HXC}}\mathrm{T} \tag{2.51}$$

accounts for changes in the density entering the SL Hamiltonian due to $\rho^{\mathrm{XC}}(x)$; $\mathrm{F}^{\mathrm{HXC}}$ is the SL Hartree-, exchange-, and correlation (HXC) kernel.

2.4 Results

2.4.1 Ionization Potentials and Fundamental Gaps

Table 2.1: Comparison of highest occupied molecular orbital (HOMO) energies (in eV) to experimental vertical ionization potentials for negatively charged atoms. G_0W_0 calculations were carried out using PBE orbitals. aug-cc-pVTZ basis sets [58, 114] were used.

	PBE	HF	G_0W_0	GKS-spRPA	Ref.
H^-	+1.5	−1.4	+0.3	−0.9	−0.75[1]
Li^-	+0.8	−0.4	−0.0	−0.8	−0.68[2]
F^-	+1.5	−4.9	−1.9	−3.2	−3.40[3]
Au^-	+0.5	−1.2	−1.7	−2.4	−2.31[4]

Comparison of the computed highest occupied molecular orbital energies to the experimental first IPs of negatively charged atoms, see Table 2.1, suggests that GKS-spRPA is substantially more accurate than G_0W_0 for negative ions, where G_0W_0 suffers from density-driven error. The GKS-spRPA highest occupied molecular orbital (HOMO) energies also improve greatly upon SL DFAs, and negative ions such as H^- are correctly bound.

For ionization potentials of neutral molecules in the GW27 benchmark [82, 119], OEP-RPA and GKS-spRPA reduce the errors by ∼50% compared to the G_0W_0 method, see Table 2.2. Both OEP-RPA and GKS-spRPA have similar mean absolute errors of ∼0.3 eV for

Table 2.2: Mean absolute (MAE), mean signed (MSE, computed−reference) and maximum absolute (Max AE) errors (eV) for highest occupied molecular orbital energies of GW27 testset [82]. For reference values, negative of the ionization potentials from CCSD(T) were used [119]. def2-TZVPP basis-sets [120] was used for CCSD (T), PBE, HF, G_0W_0 and GKS-spRPA. For comparison, OEP-RPA results from Ref. [71] using aug-cc-pCVTZ basis-sets [121] are also shown. For G_0W_0 and GKS-spRPA, the exchange-correlation potential was approximated using the PBE functional.

Error Measure	PBE [5]	HF	G_0W_0[6]	OEP-RPA [7]	GKS-spRPA
MAE	3.83	0.65	0.64	0.26	0.30
MSE	3.83	−0.31	0.64	−0.08	−0.29
Max AE	6.49	2.22	1.29	0.84	0.68

the GW27 testset. The mean signed errors show that GKS-spRPA ionization potentials are systematically too large, whereas the OEP-RPA HOMO energies can be too small or too large, as is also reflected in higher maximum absolute deviations.

OEP-RPA and GKS-spRPA quasiparticle energies differ substantially for HOMO-LUMO gaps, see Table 2.3: OEP-RPA HOMO-LUMO gaps do not contain derivative discontinuities since they come from a local KS potential [122], and substantially underestimate fundamental gaps. G_0W_0 and GKS-spRPA, on the other hand, yield fundamental gaps within 1 eV of the coupled cluster reference results for unpolar molecules. For the highly polar tetracyanoethylene molecule, G_0W_0 and GKS-spRPA underestimate the fundamental gap by 3.3 and 1.7 eV, respectively, which may indicate residual self-interaction error.

Table 2.3: Gaps (in eV) obtained as differences between the lowest unoccupied and highest occupied molecular orbital energies, and reference fundamental gaps computed using differences of CCSD(T) total energies. CCSD(T), GKS-spRPA and G_0W_0 calculations use aug-cc-pVTZ basis-sets while OEP-RPA results [71] were obtained using aug-cc-pCVTZ basis-sets [121]. For GKS-spRPA, the exchange-correlation potential is approximated using the PBE functional.

	OEP-RPA[8]	G_0W_0	GKS-spRPA	CCSD(T)
Li_2	1.23	4.43	5.28	4.76
Na_2	1.18	4.35	4.98	4.48
LiH	2.94	6.92	7.66	7.67
CH_3NO_2		9.82	11.48	11.41
$C_2(CN)_4$		6.96	8.48	10.29

2.4.2 Noncovalent Interactions

GKS-spRPA substantially reduces the underbinding error observed in SL-RPA calculations of weakly interacting noble gas dimers and the dimers of S22 dataset [123], see Figs. S1 and S2.

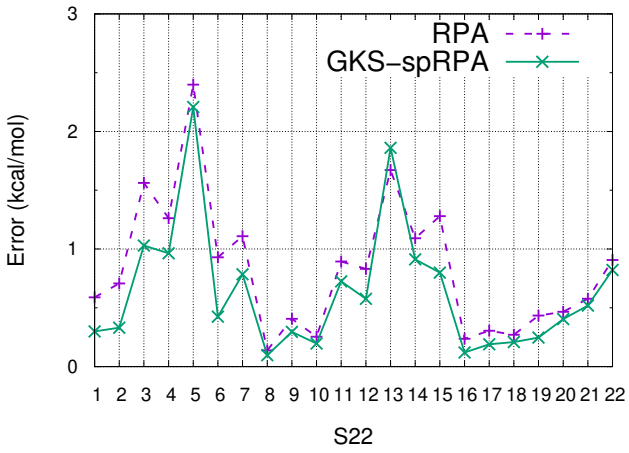

Figure 2.1: Errors (computed−reference [124]) in binding energies for the dimers of S22 dataset. The PBE XC potential and aug-cc-pwCV(T,Q)Z[125] basis set extrapolation were used.

While RPA based on PBE [7] orbitals (RPA-PBE) produces hardly any binding for He_2 and substantially underbinds Ne_2, the nuclear potential energy curves obtained from GKS-spRPA closely resemble those obtained from the coupled cluster singles doubles with perturbative triples (CCSD(T)) [132] method, which is nearly exact for these systems.

Perturbative expansion of the GKS-spRPA energy around the SL ground state provides a rationale for the significant accuracy gains upon variational optimization for weak intermolecular interactions: The lowest-order total energy change in $\|\mathrm{H}_0^{\mathrm{spRPA}} - \mathrm{H}_0^{\mathrm{SL}}\|$ is

$$E^{(2)} = \sum_{ij\lambda\lambda'} (n_\lambda - n_{\lambda'}) \frac{|\langle \phi_{i\lambda}^{\mathrm{SL}} | \mathrm{H}_0^{\mathrm{spRPA}} - \mathrm{H}_0^{\mathrm{SL}} | \phi_{j\lambda'}^{\mathrm{SL}} \rangle|^2}{\epsilon_{i\lambda}^{\mathrm{SL}} - \epsilon_{j\lambda'}^{\mathrm{SL}}}. \tag{2.52}$$

The exchange portion of $\mathrm{H}_0^{\mathrm{spRPA}} - \mathrm{H}_0^{\mathrm{SL}}$ gives rise to the "single excitations" correction to

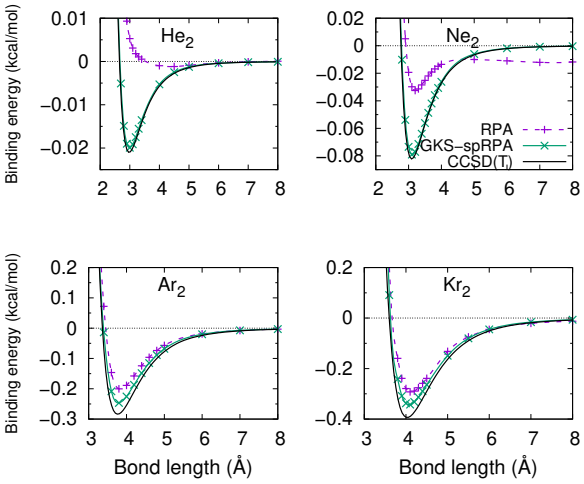

Figure 2.2: Computed PECs of noble gas dimers compared to reference data [126–129]. aug-cc-pV6Z[130] basis sets were used for He_2, Ne_2 and Ar_2, and aug-cc-pV5Z[58, 131] basis sets were used for Kr_2; an additional set of atomic basis mid-bond functions was employed to speed up basis set convergence. The PBE XC potential was used.

SL-RPA, which were shown to be important for noncovalent bonding by Ren and co-workers [133]. Replacing the SL orbitals and orbital energies in Eq. (2.52) with the GKS-spRPA ones obtained in the first iteration corresponds to the "renormalized single excitations" (rSE) correction [87] plus additional correlation-relaxation contributions. While the rSE approach also improves considerably upon SL-RPA for noble-gas dimers, it spuriously overbinds in cases such as Ne_2 [87], whereas GKS-spRPA remains accurate, reflecting the additional stability resulting from variational optimization. Similar to orbital optimized RPA [74], GKS-spRPA thus implicitly accounts for singles corrections to all orders. A comparison of equilibrium properties for Ar_2 and Kr_2 and mean average errors for binding energies of S22 dataset shows that the GKS-spRPA improves upon both SL-RPA and OEP-RPA, see Table. 2.4.

Table 2.4: Comparison of SL-RPA, OEP-RPA and GKS-spRPA results for molecular equilibrium properties (bond lengths, r_e, in Å and binding energies, D_e, in kcal/mol), as well as mean absolute errors (MAEs) in binding energies of dimers in the S22 benchmark [123]. For SL-RPA and GKS-spRPA, the exchange-correlation potential was approximated using the PBE functional. Negative binding energies indicate bound states.

	Reference			
	SL	OEP [9]	GKS sp	Expt.
Ar_2				
r_e (Å)	3.84	3.85	3.79	3.775 [128]
D_e (kcal/mol)	−0.201	−0.193	−0.247	−0.284 [128]
Kr_2				
r_e (Å)	4.12	4.13	4.07	4.06 [129]
D_e (kcal/mol)	−0.293	−0.299	−0.343	−0.393 [129]
Be_2				
r_e (Å)	2.40	2.52	2.45	2.45 [134]
D_e (kcal/mol)	−1.018	+0.498	−1.911	−2.67 [134]
S22				
MAE (kcal/mol)	0.83	1.08	0.64	

Table 2.5: Mean absolute (MAE), mean signed (MSE, computed−reference), and maximum absolute (Max AE) errors in kcal/mol for SL-RPA and GKS-spRPA using the G21 AE [135] and HEAT [12] atomization energy benchmarks. RPA and GKS-spRPA correlation energies were obtained using cc-pV(Q-5)Z[58] extrapolation for the G21 AE set, and using aug-cc-pV(Q-5)Z[58, 131] extrapolation for HEAT. Core orbitals with energies below −3 Hartree were frozen, and the exchange-correlation potential was approximated using the PBE functional.

Benchmark	Error Measure	RPA	GKS-spRPA
G21 AE	MAE	9.08	8.92
	MSE	−9.08	−8.84
	Max AE	25.39	25.43
HEAT	MAE	10.09	10.01
	MSE	−10.09	−10.01
	Max AE	25.81	24.77

2.4.3 Covalent Bonding

Compared to SL-RPA, GKS-spRPA reduces errors in atomization energies marginally but systematically for nearly all molecules contained in the G21 [135] and HEAT [12] atomization energy benchmarks. The mean absolute errors of SL-RPA and GKS-spRPA for binding

energies of covalently bound molecules are within ~ 0.1 kcal/mol of each other, see Table 2.5 and SI. This result reflects the accuracy of SL orbitals for covalent bonds. Orbital optimization using OEP-RPA, on the other hand, tends to worsen errors in reaction energies [71].

Table 2.6: Reference values and deviations Δ from CCSD(T) in kcal/mol for the G21 AE atomization energy benchmark.[135] The energies were obtained using cc-pV(Q-5)Z[58] extrapolation, core orbitals with energies below -3 Hartree were frozen, and the exchange-correlation potential was approximated using the PBE functional.

molecule	CCSD(T)	Δ(RPA)	Δ(GKS-spRPA)
LiH	57.7	-1.24	-1.03
BeH.doublet	50.1	0.02	0.36
CH.doublet	83.8	-2.52	-2.58
CH_2.triplet	189.7	-9.76	-10.45
CH_2	180.4	-5.35	-5.19
CH_3.doublet	306	-11.13	-11.71
CH4	418.7	-13.43	-13.77
NH.triplet	82.6	-0.09	-0.06
NH_2.doublet	181.6	-2.07	-2.08
NH_3	296.6	-5.38	-5.56
OH.doublet	106.7	-2.95	-3.19
H_2O	232.1	-8.19	-8.79
HF	141.1	-8.09	-8.80
SiH_2	153.9	-4.72	-4.19
SiH_2.triplet	133.5	-5.65	-5.42
SiH_3.doublet	228.7	-7.39	-6.48
SiH_4	324.3	-8.40	-6.76
PH_2.doublet	154	-0.62	-0.21
PH_3	241.6	-2.62	-1.27

H_2S	183.7	−6.38	−6.54
HCl	107.4	−6.64	−7.91
Li_2	24.1	−5.04	−4.48
LiF	137.7	−8.44	−7.67
C_2H_2	402.1	−20.90	−21.34
C_2H_4	560.7	−22.98	−23.05
C_2H_6	709.8	−25.39	−25.43
CN.doublet	177.3	−5.15	−4.62
HCN	310.4	−11.70	−11.39
CO	257.8	−13.47	−13.24
HCO.doublet	277.1	−13.49	−13.11
H_2CO	372.2	−16.47	−15.57
H_3COH	510.9	−19.46	−19.06
N_2	226.1	−3.09	−2.37
N_2H_4	435.7	−8.29	−7.59
NO.doublet	150.7	−2.89	−2.04
O_2.triplet	119.9	−6.74	−7.08
H_2O_2	267.5	−10.93	−11.16
F_2	38.2	−7.96	−8.36
CO_2	386.7	−22.36	−20.58
Na_2	16.7	−0.05	−0.22
Si_2.triplet	76.2	−10.44	−10.62
P_2	115.7	−0.19	1.38
S_2.triplet	103.8	6.69	−7.01
Cl_2	60.1	−10.30	−11.74
NaCl	99.3	−4.37	−4.84
SiO	192	−11.54	−10.31

CS	170.9	−10.51	−10.45
SO.triplet	125.7	−7.86	−7.46
ClO.doublet	64.8	−6.27	−6.78
ClF	62.6	−9.77	−9.93
Si_2H_6	535	−16.40	−13.25
CH_3Cl	394.6	−18.07	−18.85
H_3CSH	472.3	−16.83	−16.64
HOCl	165.6	−10.67	−11.27
SO_2	262.1	−21.93	−19.14
MAE		9.08	8.92

Table 2.7: Reference values and deviations Δ from CCSDTQ in kcal/mol for the HEAT atomization energy benchmark [12]. The energies were obtained using aug-cc-pV(Q-5)Z[58, 131] extrapolation, core orbitals with energies below −3 Hartree were frozen, and the exchange-correlation potential was approximated using the PBE functional.

molecule	CCSDTQ	Δ(RPA)	Δ(GKS-spRPA)
N_2	228.41	−5.21	−4.58
H_2	109.52	−0.65	−0.94
F_2	38.99	−8.59	−9.09
O_2	120.77	−7.70	−8.13
CO	259.13	−14.81	−14.68
C_2H_2	405.45	−24.48	−24.77
C_2H	266.07	−21.66	−21.84
CH_2	190.81	−11.04	−11.70
CH	84.22	−2.93	−2.99
CH_3	307.95	−13.26	−13.83

CO_2	390.15	−25.81	−24.29
H_2O_2	269.2	−13.24	−13.43
H_2O	233.13	−9.63	−10.14
HCO	279.30	−15.75	−15.44
HF	141.65	−9.01	−9.62
HO2	175.53	−9.57	−9.52
NO	152.62	−4.90	−4.13
OH	107.28	−3.76	−3.93
HNO	205.82	−6.80	−5.68
CN	181.07	−8.83	−8.39
HCN	313.32	−14.57	−14.34
CF	132.77	−12.42	−11.42
NH2	182.65	−3.27	−3.26
NH_3	298.16	−7.29	−7.44
NH	83.12	−0.68	0.62
OF	52.95	−6.76	−6.16
MAE		10.09	10.01

2.4.4 Beryllium Dimer

The potential energy curve (PEC) of beryllium dimer is a stringent test for approximate electron correlation theories, because it requires an accurate description of long-range dispersion interactions and strong near-degeneracy correlation between low-lying excited ^1P states of the isolated Be atoms [136]. The HF PEC is repulsive, second-order Møller-Plesset

perturbation (MP2) theory produces binding energies nearly 3 times too small compared to experiment, while those from local and SL density functional theory are 3-5 times too large [137, 138]. Some of the SL functionals also display a small unphysical maximum. RPA-PBE produces too shallow well depth and an unphysical repulsive barrier at intermediate bonding distances, see Fig. 2.3, which neither the perturbative rSE correction nor second order screened exchange (SOSEX) correct entirely [33, 139, 140]. However, the combination of these corrections, i.e. RPA-PBE+rSE+SOSEX, removes this unphysical barrier [33]. OEP-RPA does not remove the barrier and produces a positive well-depth, i.e., Be_2 is unbound within OEP-RPA, see Fig. 2.3 and Table 2.4. GKS-spRPA not only removes the unphysical barrier, but also considerably improves the well-depth, yielding results close to the CCSD(T) ones. As CCSD(T) calculations are approximately 2 orders of magnitude more costly than GKS-spRPA calculations for many applications, this is a significant result, even though both methods fall short of capturing the strong static correlation at short bond distances.

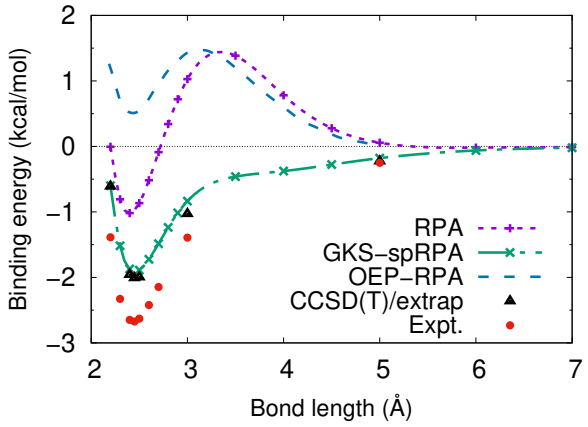

Figure 2.3: Computed GKS-spRPA aug-cc-pwCV5Z [141] PECs of Be_2 molecule compared to OEP-RPA (using plane-wave basis sets with 50 Ry cutoff) [70], experiment [134] and complete basis-set limit CCSD(T) [142].

2.5 Conclusions

OSC optimization of approximate XC energy functionals with an explicit dependence on the KS potential requires specification of the KS potential as functional of the density and/or the KS orbitals and occupation numbers. However, most choices, including the so-called "exact" KS potential, produce an inconsistency between the KS potential and the functional derivative of the thus defined energy expression. Equivalently, the KS density used to evaluate the energy functional differs from the presumably more accurate Hellmann-Feynman density. This paradox appears to have been overlooked previously, and casts doubt onto OSC schemes for explicitly potential-dependent functionals such as OEP-RPA and OEP-based many-body perturbation theory.

This paradox is resolved by imposing the exact constraint on the KS potential that it must stationarize a given approximate XC energy functional at fixed KS orbitals and occupation numbers. If this condition uniquely determines the KS potential, this FSC potential is optimal in the sense that it is consistent with the energy functional it defines, and the resulting KS density equals the Hellmann-Feynman density. The FSC condition is a constraint on the KS potential and as such distinct from the OSC variational principle or OEP methods. If this condition gives rise to a unique KS potential, it provides a more consistent definition of the mapping between the KS potential and the best available approximation to the interacting density than the "exact" KS potential.

The GKS-spRPA scheme implements the FSC condition approximately, by requiring the GKS potentials defining the energy and obtained from its functional derivative to have the same ground state density matrix (and, equivalently, GKS determinant). Our results show that GKS-spRPA overcomes major limitations of SL DFAs and SL-RPA resulting from density-driven error: Negative ions are bound when they should be, and noncovalent interaction energies are significantly improved. GKS-spRPA covalent binding energies are

only slightly more accurate than the SL-RPA ones, but the improvement is very systematic, as expected for a well-defined OSC variational approach. Errors previously attributed to missing beyond-RPA correlation, such as the spurious maximum in the Be PEC [33, 140] or inaccurate energy differences [104] vanish upon GKS optimization, suggesting that they may be primarily caused by lacking variational stability and functional selfconsistency rather than inherent errors of the RPA method.

The GKS-spRPA orbital energies match experimental ionization potentials and electron affinities of atoms and molecules within a few tenths of an eV, surpassing the popular G_0W_0 method in accuracy. Analysis of the nonlocal GKS-spRPA correlation potential supports these observations, showing that quasiparticle GW energies are a first-order perturbative limit of canonical GKS-spRPA orbital energies. Unlike KS band gaps, the GKS-spRPA band gaps contain the energy derivative discontinuity at integer particle numbers, and thus accurately approximate the observable fundamental gap; this is of particular interest for infinite systems such as periodic solids, where IPs cannot be obtained from total energy differences.

The GKS-spRPA GKS solution is considerably more resilient to symmetry breaking than OSC SL KS solutions, as suggested by the location of the Coulson–Fischer point for the H_2 ground state. Moreover, GKS-spRPA eliminates the spurious second Coulson–Fischer point observed in non-OSC SL-RPA approaches. In conjunction with the above results, these improved stability characteristics provide additional evidence for the viability and robustness of the GKS-spRPA energy functional. In particular, the high stability of the GKS-spRPA solution bodes well for applications to response properties, whose accuracy can sensitively depend on the stability of the reference state.

From a computational viewpoint, the cost of a GKS-spRPA is on the order of that of a SL-RPA calculation times the number of GKS iterations; thus, GKS-spRPA calculations for systems with hundreds of atoms are within reach. KS-spRPA is considerably less costly

than OEP-RPA, because it does not require ad-hoc regularization or special basis sets, and it is relatively straightforward to implement starting from RPA analytical gradients. While GKS-spRPA does not achieve complete functional selfconsistency, its considerably improved performance for energy differences and density-related properties compared to both SL RPA and OEP-RPA suggests that semicanonical projection provides a simple yet relatively accurate approximation to the FSC RPA potential.

The GKS scheme with semicanonical projection presented here may be applied beyond RPA to turn any conserving [143–145] energy functional of the KS one-particle Green's function into a density functional, and provides a solution to the conundrum of how to obtain accurate energy differences and choose the non-interacting system, e.g., in GW theory [146]: *All* observables, such as self-energies or response properties, are obtained as derivatives of a single, variationally stable energy functional of the KS density matrix, combining and enhancing the accuracy of RPA for energetics with the one of GW for quasiparticle spectra. Thus, GKS-spRPA is a step towards accurate, efficient, and universal electronic structure methods sharing favorable characteristics of both DFT and GFT.

Chapter 3

Static polarizabilities within the GKS-spRPA

This chapter contains verbatim excerpts from a manuscript under preparation titled "Static polarizabilities within the generalized Kohn–Sham semicanonical projected random phase approximation (GKS-spRPA)", reprinted with permission, from S. G. Balasubramani, V. K. Voora and F. Furche. This material is based upon work supported by the National Science Foundation under CHE−1464828 and CHE−1800431.

3.1 Introduction

Technologically advanced optical and optoelectronic devices such as organic light emitting diodes [147], organic liquid crystal displays [148] are often based on π-conjugated molecules [149] that have large optical response properties such as polarizabilities ($\boldsymbol{\alpha}$) and hyperpolarizabilities ($\boldsymbol{\beta}$). Theoretical calculations that help guide experimental design of such molecules with tailored (non)linear optical response properties [2] would help speed up materials discovery. Density functional theory (DFT) [4, 150] within the Kohn–Sham (KS) [5] or the generalized KS (GKS) [86] framework has been the workhorse for computations of higher-order molecular properties[151, 152] because of the cheap computational cost and reasonable accuracy. However, the electronic structure of systems such as transition metal complexes, metal clusters with small-gaps and π-conjugated molecules are not accurately described by popular density functional approximations (DFAs) such as PBE and B3-LYP.

Champagne and coworkers [17, 153, 154] have systematically assessed the use of semilocal (SL) and hybrid density functional approximations (DFAs) for the calculations of polarizabilities and hyperpolarizabilities. They found large overestimations of the (hyper)polarizabilities of π-conjugated oligomers using SL functionals. This was initially attributed to the wrong exponential asymptotic decay of the KS potential, however, long-range corrected functionals did not provide substantial improvements. [153] Recent studies using (optimally tuned) range-separated hybrids (RSHs) for calculating (hyper)polarizabilities have reported improved results compared to SL DFAs but contain adjustable parameters which limit their predictive power. [155–157] Scuseria and coworkers [158] noted that the inclusion of large fractions of HF exchange appeared to be the reason for the success of various RSHs [158]. Champagne and coworkers [155] have argued that not only long-range exchange but long-range correlations are also important for obtaining accurate polarizabilities of these conjugated systems. Champagne and coworkers also used wave function based methods such as Hartree-Fock (HF), nth-order Møller-Plesset perturbation theory (MPn) and coupled cluster

theory (CC) to analyze the polarizabilities of conjugated molecules. [159] They used the 6-31G basis set for calculations involving MP2, MP4 and CCSD(T), whereas Oviedo et al. used the cc-pVDZ basis set for their calculations of static polarizabilities of polydiacetylene (PDA) and polybutatriene (PBT) oligomers with the CCSD(T)-F12 method. [156] These small basis sets are insufficient to obtain converged static polarizabilities [160] and using larger basis sets is not practical for calculations involving methods such as CC since their computational cost scales undesirably with system size ($\mathcal{O}(N^5)$ or larger). These studies lead to the following question: can one obtain molecular properties using a method that contains both nonlocal exchange and nonlocal correlation from first principles with a computational cost of $\leq \mathcal{O}(N^5)$, and if so, would that solve the problems faced by SL/hybrid and RSH DFAs for these π-conjugated systems?

To answer these questions, we consider here the random phase approximation (RPA) [20–22, 28, 161], which is the simplest post-KS DFA based on the adiabatic-connection fluctuation-dissipation theorem (ACFDT). [19, 29, 108, 162] Post-KS RPA is a parameter-free DFA that is compatible with HF exchange and seamlessly includes van der Waals interactions. [30] The first molecular tests of post-KS RPA for calculating ground state energies using finite basis sets were carried out in 2001 [31], and in the following two decades RPA has been implemented in many electronic structure program packages and tested on several molecular and extended systems [32–34, 163–165].

The computational scaling of post-KS RPA, using the resolution of identity (RI) approximation [166–168] and imaginary frequency integration is $\mathcal{O}(N^4 \log(N))$, with system size N. [35] Post-KS RPA has been shown to work well for systems with a small- or even zero-gap, such as extended systems [169], metal clusters [34], transition metal compounds [170] and it has been extensively benchmarked for dispersion interactions of large, noncovalently interacting complexes, where it performs much better than the second-order Møller–Plesset perturbation theory (MP2) [36, 37] and SL/hybrid DFAs. [171]

Analytical molecular first-order properties within the post-KS RPA were efficiently implemented and tested by Burow et al. [43] Upon extensive benchmarking, they concluded that the post-KS RPA predicted molecular geometries more accurately than MP2 and semilocal/hybrid DFAs especially for van der Waals complexes and transition metal compounds. They also reported vibrational frequencies, which are second-order properties, that they had obtained using numerical finite differences of the analytical gradients.

Numerical energy derivatives can be straightforward to implement but are prone to instabilities and are not very resource efficient. [45, 172] Analytical derivatives however, are algorithmically tedious to implement but are robust, [173, 174] provide a direct method for calculating molecular properties and are usually preferred over numerical schemes. [48, 175–179]

Here, we present the very first analytical implementation of $\boldsymbol{\alpha}(0)$ within the newly developed orbital self-consistent GKS semicanonical projected RPA (GKS-spRPA) [180] and benchmark the accuracy of its linear response properties. Specifically, we aim to understand if GKS-spRPA, which includes HF exchange as well as long-range nonlocal correlations, can address the problem of overpolarization faced by SL/hybrid DFAs for calculations of $\boldsymbol{\alpha}(0)$ of $\pi-$conjugated polymers. Furthermore we test the accuracy of GKS-spRPA $\boldsymbol{\alpha}(0)$ for metallocenes and small metal clusters where HF is qualitatively incorrect and MP2 is not very accurate. [181, 182]

This chapter is organized as follows: in section 3.2 we briefly review the GKS-spRPA theory as well as set up the notations and define some intermediates that will be used in the remainder of the manuscript. Next, we introduce the variational Lagrangian along with the GKS-spRPA Fock matrix. The intermediates that are required to build both the first-order Fock matrix as well as the right hand side are derived and some strategies for efficient implementation are discussed. In section 3.3 the implemented GKS-spRPA static polarizabilities are tested on a wide range of molecular systems. Furthermore, the basis set and numerical

frequency grid convergence behavior of the method are discussed. Finally, in section 3.4 we provide conclusions.

3.2 Theory

3.2.1 Review of the GKS-spRPA

In this manuscript, we use the standard notations to denote orbital indices which are as follows, occupied: $\{i, j, k, l, \ldots\}$, virtual: $\{a, b, c, d, \ldots\}$, general: $\{p, q, r, s, \ldots\}$, atomic: $\{\mu, \nu, \kappa, \lambda, \ldots\}$ and auxillary: $\{\mathcal{P}, \mathcal{Q}, \mathcal{R}, \mathcal{S}, \ldots\}$. $\{\phi_p(x)\}$ denotes molecular orbitals(MOs), $\{\chi_\mu(\mathbf{r})\}$ denotes atomic orbitals (AOs) and $x = \{\mathbf{r}, \sigma\}$ denotes the space-spin coordinates. The AOs and MOs are related through the MO coefficients

$$\phi_{p,\sigma}(x) = \sum_{\mu} C^{p}_{\mu,\sigma} \chi_\mu(\mathbf{r}). \tag{3.1}$$

The one particle (spin-unrestricted) density matrix and the AO overlap matrix are given by

$$\mathrm{D}_{\mu\nu,\sigma} = \sum_{i} C^{i}_{\mu,\sigma} C^{i*}_{\nu,\sigma} \tag{3.2}$$

$$\mathrm{S}_{\mu\nu} = \int d\mathbf{r}\ \chi_\mu(\mathbf{r}) \chi_\nu(\mathbf{r}). \tag{3.3}$$

For post-KS energy functionals such as the RPA, the reference (semi)local KS orbitals and orbital energies are obtained as the solution of

$$\mathbf{H}^{\mathrm{KS}}_{\sigma} \mathbf{C}_\sigma = \boldsymbol{\epsilon}_\sigma \mathbf{S} \mathbf{C}_\sigma \tag{3.4}$$

where the KS Hamiltonian can be separated into a one electron part $\boldsymbol{h}$, the Hartree or

Coulomb potential $\mathbf{V}^{\mathrm{H}}$ and the exchange-correlation potential $\mathbf{V}^{\mathrm{XC}}$ as

$$\mathrm{H}^{\mathrm{KS}}_{pq,\sigma} = h_{pq,\sigma} + \sum_{rs,\sigma'} \mathrm{V}^{\mathrm{H}}_{pr\sigma qs\sigma'} \mathrm{D}_{rs,\sigma'} + \mathrm{V}^{\mathrm{XC}}_{pq,\sigma'}[\mathbf{D}] \tag{3.5}$$

Consider orthogonal semicanonical projection operators $\hat{\mathbf{P}}$ which project onto the occupied-occupied and virtual-virtual diagonal blocks of the KS Hamiltonian

$$\tilde{\mathbf{H}} = \hat{\mathbf{P}}\mathbf{H}^{\mathrm{KS}}\hat{\mathbf{P}}. \tag{3.6}$$

The spRPA energy functional employing the resolution of identity (RI) approximation[166, 167] can be expressed as a functional of the density matrix $\mathbf{D}$ and the semicanonical projected KS Hamiltonian $\tilde{\mathbf{H}}$ as

$$E^{\mathrm{spRPA}}[\mathbf{D}, \tilde{\mathbf{H}}] = E^{\mathrm{HF}}[\mathbf{D}] + E^{\mathrm{C\ spRPA}}[\mathbf{D}, \tilde{\mathbf{H}}], \tag{3.7}$$

$$E^{\mathrm{C\ spRPA}} = \frac{1}{2}\int_{\infty}^{\infty} \frac{d\omega}{2\pi} \langle \ln\left(\mathbb{1} + \mathbf{Q}(\omega)\right) - \mathbf{Q}(\omega) \rangle, \tag{3.8}$$

where $\langle . \rangle$ denotes the trace operation. $\mathbf{Q}(\omega)$ can be expressed in the RI basis as

$$\mathrm{Q}_{\mathcal{P}\mathcal{Q}}(\omega) = \sum_{ia,\sigma} B_{\mathcal{P}ai\sigma} \frac{(\epsilon_{a\sigma} - \epsilon_{i\sigma})}{\omega^2 + (\epsilon_{a\sigma} - \epsilon_{i\sigma})^2} B_{ia\sigma\mathcal{Q}}, \tag{3.9}$$

where the RI factorized [166, 167] two electron integrals (Mulliken notation) are

$$\begin{aligned} (ia|jb) &\approx \sum_{\mathcal{P}\mathcal{Q}} (ia|\mathcal{P})(\mathcal{P}|\mathcal{Q})^{-1}(\mathcal{Q}|jb) = \sum_{\mathcal{R}} B_{ia\mathcal{R}} B_{\mathcal{R}jb}; \\ B_{ia\mathcal{R}} &= \sum_{Q} (ia|\mathcal{Q})(\mathcal{Q}|\mathcal{R})^{-1/2}. \end{aligned} \tag{3.10}$$

The GKS-spRPA Hamiltonian is obtained as

$$\mathbf{H}^{\text{GKS-spRPA}} = \frac{\delta E^{\mathrm{spRPA}}}{\delta \mathbf{D}^T} = \mathbf{H}^{\mathrm{HF}} + \mathbf{V}^{\mathrm{c\ GKS\text{-}spRPA}}. \tag{3.11}$$

The occupied-virtual block of $\mathbf{H}^{\text{GKS-spRPA}}$ (here after denoted $\mathbf{H}^{\text{RPA}}$ for sake of brevity) is

$$\mathrm{H}_{ia}^{\text{RPA}} = 2\mathrm{H}_{ia}^{\text{HF}} + \gamma_{ia} - \gamma_{ai} + \mathrm{H}_{ia}^{+}[\mathbf{T}] + [\mathbf{T}, \mathbf{H}^{\text{KS}}]_{ia}, \tag{3.12}$$

where

$$\mathrm{H}_{\mu\nu\kappa\lambda}^{+} = \frac{\delta \mathrm{V}_{\mu\nu}^{\text{HXC}}}{\delta D_{\kappa\lambda}}, \tag{3.13}$$

is the Hartree-exchange-correlation kernel, $\mathbf{T}$ is the RPA unrelaxed difference density matrix defined as

$$\mathbf{T} = \frac{\delta E^{\text{C spRPA}}}{\delta \tilde{\mathbf{H}}_0^T}, \tag{3.14}$$

and the $\boldsymbol{\gamma}$ is defined as

$$\gamma_{pq} = \sum_{\mu} \frac{\partial E^{\text{C spRPA}}}{\partial C_{\mu}^{p}} C_{\mu}^{q}. \tag{3.15}$$

Detailed expressions for $\boldsymbol{\gamma}$ and $\mathbf{T}$ are given in Appendix A.1. The condition for the GKS-spRPA orbital self consistency is $\mathbf{H}_{ov}^{\text{RPA}} = \mathbf{0}$ and the algorithm is provided in the supporting information. This self consistent scheme can be extended to other post KS energy functionals such as the AXK[42], SOSEX[41], rPT2[87], etc.

3.2.2 The Energy Lagrangian

The variational principle is key for the computation of higher order molecular properties as derivatives of the energy Lagrangian. The $2n+1$ and $2n+2$ rules for the variational parameters and Lagrange multipliers respectively, can be employed for the n^{th} order derivative[47]. The GKS-spRPA energy functional is invariant under occupied-occupied and virtual-virtual

orbital rotations. [180] For such energy functionals, a convenient way to express variations with respect to orbital coefficients is through the anti-Hermitian orbital rotation matrix $\boldsymbol{\varkappa}$. [183] Thus, a change of variable can be made from $\boldsymbol{C}$ to $\boldsymbol{\varkappa}$ and for example the occupied MO coefficients can be expressed as

$$C_\mu^i(\boldsymbol{\varkappa}) = C_\mu^i(0) + \sum_a \varkappa_{ia} C_\mu^a(0) + \dots \tag{3.16}$$

More details about derivatives with respect to $\boldsymbol{\varkappa}$ can be found in the supporting information. The GKS-spRPA energy Lagrangian (GKS-spRPA will be denoted as RPA unless mentioned otherwise for sake of brevity) can be expressed as

$$\begin{aligned} &L^{\mathrm{RPA}}(\boldsymbol{\varkappa}, \boldsymbol{\varepsilon}, \boldsymbol{\mathcal{T}}, \boldsymbol{\mathcal{W}} | \mathbf{S}, \mathbf{V}^{\mathrm{xc}}, \mathbf{X}) = E^{\mathrm{RPA}}(\boldsymbol{\varkappa}, \boldsymbol{\varepsilon} | \mathbf{X}) \\ &+ \sum_{\sigma,ij} \left(\mathcal{T}_{ij,\sigma} (\mathrm{H}^{\mathrm{KS}}_{ij,\sigma} - \boldsymbol{\varepsilon}_{ij,\sigma} \delta_{ij}) \right) + \sum_{\sigma,ab} \left(\mathcal{T}_{ab,\sigma} (\mathrm{H}^{\mathrm{KS}}_{ab,\sigma} - \boldsymbol{\varepsilon}_{ab,\sigma} \delta_{ab}) \right) \\ &- \sum_{\sigma,pq} \left(\mathcal{W}_{pq,\sigma} (S_{pq,\sigma} - \mathbb{1}_{pa}) \right) \end{aligned} \tag{3.17}$$

where the Lagrange multipliers $\boldsymbol{\mathcal{T}}$ is the RPA unrelaxed difference density matrix and the $\boldsymbol{\mathcal{W}}$ is the energy weighted density matrix. The variational parameters are the semicanonical KS orbital energies $\boldsymbol{\varepsilon}$ and the orbital rotation matrix $\boldsymbol{\varkappa}$. The one electron Hamiltonian and the two, three and four index electron repulsion integrals can be compactly written as a set $\mathbf{X} = \{\boldsymbol{h}, (\mathcal{P}|\mathcal{Q}), (ia|\mathcal{P}), (ia|jb)\}$. [35, 184] $\boldsymbol{\varkappa}$ and $\boldsymbol{\varepsilon}$ parametrically depend on $\mathbf{S}$, $\mathbf{V}^{xc}$ and $\mathbf{X}$. The Lagrangian (L and L^{RPA} are used interchangeably to denote the GKS-spRPA energy Lagrangian) is required to satisfy stationarity with respect to the multipliers and the variational parameters,

$$\left.\frac{\partial L}{\partial \boldsymbol{\varkappa}}\right|_{stat} = \left.\frac{\partial L}{\partial \boldsymbol{\mathcal{W}}}\right|_{stat} = \left.\frac{\partial L}{\partial \boldsymbol{\mathcal{T}}}\right|_{stat} = \left.\frac{\partial L}{\partial \boldsymbol{\varepsilon}}\right|_{stat} = \mathbf{0}. \tag{3.18}$$

At the stationary point the optimized parameters and multipliers are denoted by $\boldsymbol{\varkappa} = \boldsymbol{\kappa},\ \boldsymbol{\mathcal{W}} = \mathbf{W},\ \boldsymbol{\varepsilon} = \boldsymbol{\epsilon},\ \boldsymbol{\mathcal{T}} = \mathbf{T}$ and we have

$$E^{\mathrm{RPA}}(\boldsymbol{\kappa}, \boldsymbol{\epsilon}|\mathbf{X}) = L^{\mathrm{RPA}}(\boldsymbol{\varkappa}, \boldsymbol{\varepsilon}, \boldsymbol{\mathcal{T}}, \boldsymbol{\mathcal{W}}|\mathbf{S}, \mathbf{X}, \mathbf{V}^{\mathrm{XC}})|_{stat} \tag{3.19}$$

Apart from the stationarity of L^{RPA} with respect to $\boldsymbol{\kappa}$, GKS-spRPA orbital self-consistency also implies that

$$\frac{dE^{\mathrm{RPA}}}{d\kappa_{ia}} = \mathrm{H}^{\mathrm{RPA}}_{ia} = 0 \tag{3.20}$$

is satisfied upon reaching self-consistency following the algorithm described in Appendix A.3.

3.2.3 Second derivatives of the GKS-spRPA energy functional

The general expression for the second derivative of the GKS-spRPA energy with respect to perturbations ζ and χ, upon satisfaction of all the stationarity conditions listed in Eqn. 3.18, can be obtained as

$$\begin{aligned}
\frac{\partial^2 E}{\partial\chi\partial\zeta} = \Bigg(&\left\langle \left(\frac{\partial^2 L}{\partial\chi\partial\boldsymbol{\kappa}}\right)\frac{\partial\boldsymbol{\kappa}}{\partial\zeta}\right\rangle + \left\langle \left(\frac{\partial^2 L}{\partial\chi\partial\boldsymbol{\epsilon}}\right)\frac{\partial\boldsymbol{\epsilon}}{\partial\zeta}\right\rangle + \left\langle \left(\frac{\partial^2 L}{\partial\chi\partial\mathbf{X}}\right)\frac{\partial\mathbf{X}}{\partial\zeta}\right\rangle \\
&+ \left\langle \left(\frac{\partial L}{\partial\mathbf{X}}\right)\frac{\partial^2\mathbf{X}}{\partial\chi\partial\zeta}\right\rangle + \left\langle \left(\frac{\partial^2 L}{\partial\chi\partial\mathbf{S}}\right)\frac{\partial\mathbf{S}}{\partial\zeta}\right\rangle + \left\langle \left(\frac{\partial L}{\partial\mathbf{S}}\right)\frac{\partial^2\mathbf{S}}{\partial\chi\partial\zeta}\right\rangle \\
&+ \left\langle \left(\frac{\partial^2 L}{\partial\chi\partial\mathbf{V}^{\mathbf{XC}}}\right)\frac{\partial\mathbf{V}^{\mathbf{XC}}}{\partial\zeta}\right\rangle + \left\langle \left(\frac{\partial L}{\partial\mathbf{V}^{\mathbf{XC}}}\right)\frac{\partial^2\mathbf{V}^{\mathbf{XC}}}{\partial\chi\partial\zeta}\right\rangle + \left\langle \left(\frac{\partial^2 L}{\partial\chi\partial\mathbf{W}}\right)\frac{\partial\mathbf{W}}{\partial\zeta}\right\rangle \Bigg)\Bigg|_{stat}
\end{aligned} \tag{3.21}$$

When χ and ζ are static electric field perturbations Eq. 3.21 refers to the static polarizability, when χ and ζ refer to nuclear displacements then Eq. 3.21 corresponds to the geometrical Hessian. In this study we are concerned with the static polarizability and the field dependence only comes in through the orbital rotation parameter $\boldsymbol{\kappa}$ and the one electron Hamiltonian $\boldsymbol{h}$. The first-order perturbed $\boldsymbol{\kappa}$ can be obtained as a solution of the linear

equation

$$\left(\frac{\partial^2 L}{\partial \boldsymbol{\kappa} \partial \boldsymbol{\kappa}}\right)\Big|_{stat} \frac{\partial \boldsymbol{\kappa}}{\partial \chi} = -\left(\frac{\partial^2 L}{\partial \chi \partial \boldsymbol{\kappa}}\right)\Big|_{stat} \tag{3.22}$$

where the term in the brackets corresponds to the symmetric part of the orbital rotation Hessian, often denoted as $(\mathbf{A}+\mathbf{B})$ in the TDDFT literature which is a supermatrix of dimensions $N_o N_v \times N_o N_v$, where N_o and N_v denote the number of occupied and virtual MOs, respectively. [185] The right hand side (RHS) of the above equation at the stationary point, can be identified as the field derivative of the *ov* block of the GKS-spRPA Hamiltonian, $\frac{\partial \mathrm{H}_{ia}^{\mathrm{RPA}}}{\partial \chi}$. The second term that contributes to the GKS-spRPA static polarizability is due to the unrelaxed difference density matrix

$$\left\langle \left(\frac{\partial^2 L}{\partial \chi \partial \boldsymbol{h}}\right)_{stat} \frac{\partial \boldsymbol{h}}{\partial \zeta} \right\rangle = \left\langle \frac{\partial \mathbf{D}^{\text{GKS-spRPA}}}{\partial \chi} \mu^{\zeta} \right\rangle, \tag{3.23}$$

where $\mathbf{D}^{\text{GKS-spRPA}} = \mathbf{D}^{\text{HF}} + \mathbf{T}$ and $\boldsymbol{\mu}^{\zeta}$ corresponds to the ζ^{th} component of the dipole moment matrix. $\mathbf{D}^{\text{HF}}$ does not explicitly depend on χ resulting in

$$\begin{aligned}\frac{\partial^2 E^{\text{RPA}}}{\partial \chi \partial \zeta} = &-\left\langle \frac{\partial \boldsymbol{\kappa}}{\partial \chi} \left(\frac{\partial^2 L}{\partial \boldsymbol{\kappa} \partial \boldsymbol{\kappa}^{\dagger}}\right)^{-1}_{stat} \frac{\partial \boldsymbol{\kappa}^{\dagger}}{\partial \zeta} \right\rangle \\ &+ \left\langle \frac{\partial \mathbf{T}}{\partial \chi} \boldsymbol{\mu}^{\zeta} \right\rangle \end{aligned} \tag{3.24}$$

Simplified expressions for the RHS and the matrix-vector product are given in Appendix A.4.5. The orbital self-consistent scheme of GKS-spRPA helps avoid the calculations of first-order orbital relaxation terms, in the computation of second-order properties, that would otherwise require solutions of costly coupled perturbed equations. Furthermore, the computational scaling of GKS-spRPA is $\mathcal{O}(N^4 log(N)$ and therefore the calculations of $\boldsymbol{\alpha}(0)$ are not that much more expensive than the calculations of RPA geometrical gradients [43].

3.2.4 Strategies for efficient implementation

The solution of the linear problem defined in Eq. 3.22 is necessary to obtain the first part of the static polarizability within the GKS-spRPA, as shown in Eq. 3.24. Large linear equations and eigenvalue problems are often encountered during molecular property calculations in quantum chemistry. [186] Since these problems can be extremely large, involving dense matrices, iterative techniques are preferred that avoid storage of the entire coefficient matrix of the linear equation and deal with only the matrix-vector products. [187] Krylov space methods have been successfully applied in molecular response theory for solving linear and eigenvalue problems. [188–190] In this study we use a recently developed nonorthonormal extension of Krylov space methods for solving Eq. 3.22, which exploits the decreasing norm of the residual vectors to boost screening in integral-direct response calculations. [52]

The construction of the matrix-vector product is the most time consuming step in solving Eq. 3.22. The matrix-vector product as well as the RHS requires zeroth-order intermediates that are calculated on the frequency grid. For example T_{ij} as defined in Eq. A.3, requires three $\mathcal{O}(N^4)$ steps to build per frequency grid point. Avoiding repetition of these zeroth-order builds is a necessary step towards an efficient algorithm and we use the following steps to achieve this.

1. Two index zeroth-order intermediates such as T_{ij}, T_{ab}, γ_{ia}, γ_{ai}, γ_{ij} and γ_{ab} are built and stored in memory. The $\mathbf{Q}$ matrix is frequency dependent and is written to file for each grid point ω_g as $\mathrm{Q}_{\mathcal{PQ}}(\omega_g)$.

2. The RHS is built with the zeroth-order intermediates from memory as well as perturbed first order intermediates. $\mathbf{T}^{\zeta}$ and $\boldsymbol{\mu}^{\chi}$ are used to get the first contribution to the polarizability as $\alpha^{\zeta\chi} = \sum_{ij} \mathrm{T}^{\zeta}_{ij}\mu^{\chi}_{ji} + \sum_{ab} \mathrm{T}^{\zeta}_{ab}\mu^{\chi}_{ba}$.

3. Starting from the guess vectors $\{\mathbf{V}^{\zeta}\}$, zeroth- and first-order intermediates, the matrix-

vector product $\{\mathbf{M}^{\zeta}\}$ is built to setup and solve the subspace linear problem.

4. The polarizability is obtained using the converged vectors and the matrix-vector product as $\alpha^{\zeta\chi} = \sum_{ia} \mathrm{M}_{ia}^{\zeta} \mathrm{V}_{ai}^{\chi}$.

3.3 Results

3.3.1 Basis set convergence of the GKS-spRPA polarizability

The basis set requirements for calculations of molecular response properties are starkly different from that of ground state energy calculations where it is sufficient to describe unperturbed molecular orbitals accurately. [191–193] In response calculations, the orbital response to perturbations need to be considered to obtain converged results, otherwise the basis set incompleteness error can be quite large typically for smaller systems. [160, 194]

The Karlsruhe def2 basis sets are polarized, segmented contracted and were developed to describe both the core and the valence electrons as well as provide excellent performance to cost ratios for large scale DFT and HF calculations [120] First we use these basis sets as the starting points in our convergence tests of the GKS-spRPA static polarizabilities and then use the property optimized basis sets developed by Rappoport and Furche[160]. These are compact augmented basis sets with few diffuse functions that were developed based on the polarizability variational principle. [160] The exponents were determined based on maximization of HF isotropic static polarizabilities and this variational maximization leads to optimal number of diffuse basis functions.

To understand the behavior of the GKS-spRPA polarizabilities with respect to the basis set size, LiF and HCN are used as test molecules. The geometries were obtained from experimental results. The basis sets used in this study include def2-SVP, TZVPP, QZVPP,

SVPD, TZVPPD and QZVPPD. The extended def2-QZVPP basis sets which are constructed by downward extrapolation from the def2-QZVPP basis sets ($1s1p1d1f$ for the elements H-Be and $1s1p1d1f1g$ for all others) as suggested by Rappoport et al.[160], were used to approximate the basis set limit. We compare the basis set convergence of GKS-spRPA with HF, PBE, PBE0, MP2 and CC2 methods, as can be seen from Fig. 3.1. The % relative

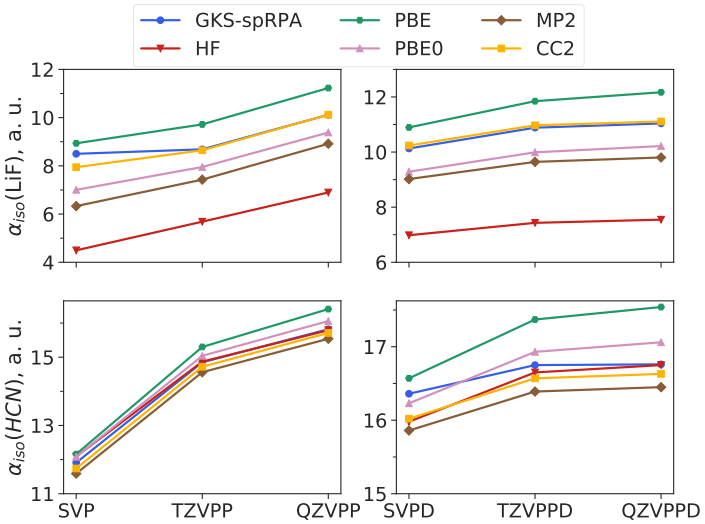

Figure 3.1: Basis set convergence of the isotropic static polarizability within the GKS-spRPA method of LiF and HCN molecules, compared to the HF, PBE, PBE0, MP2 and CC2 methods.

deviation (%RD $= \frac{(\alpha^{method} - \alpha^{reference})}{\alpha^{reference}} \times 100$) in the isotropic static polarizability of LiF using the basis sets def2-SVP, TZVPP, QZVPP, SVPD, TZVPPD and QZVPPD are 23%, 21%, 8%, 8%, 1% and 0.4% respectively. For he HCN molecule the %RD for the same order of basis sets are 29%, 12%, 6%, 3%, 0.74% and 0.71%, respectively. The def2-QZVPPD basis set produces %RD of $\leq 0.7\%$, while the def2-TZVPPD basis set results in $\leq 1\%$ RD compared to the basis set limit in these test calculations. From this analysis it is concluded that these basis sets are well suited for calculations of static polarizabilities using the GKS-spRPA method.

3.3.2 Convergence with the number of frequency grid points

The matrix-vector product and the right hand side builds of Eq. 3.22 require intermediates that are computed by integration over imaginary frequency. This is done numerically using the Clenshaw-Curtis quadrature with a finite number of grid points as described by Eshuis et al. [35], who used it for computing the RIRPA correlation energy.

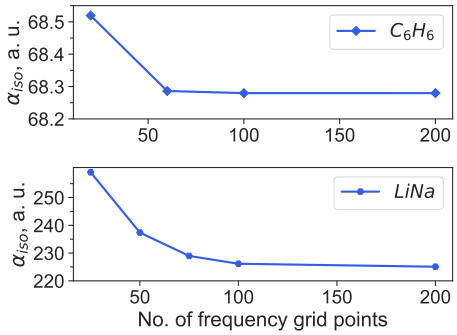

Figure 3.2: The convergence of the isotropic polarizability within the GKS-spRPA method as a function of the number of frequency grid points for benzene (top) and LiNa (bottom) molecules using the def2-QZVPPD basis and the PBE input orbitals and orbital energies.

To test the convergence of the GKS-spRPA static polarizabilities with the number of frequency grid points, we chose to study the C_6H_6 and LiNa molecules. The geometries of these molecules were optimized at the level of B3-LYP DFA, the cc-pVTZ basis set, m4 integration grid, scf convergence threshold of 10^{-8} and the optimized geometries are provided in the supporting information. The results of GKS-spRPA static polarizabilities calculated with the def2-QZVPPD basis set and the PBE semilocal input as a function of the number of frequency grid points are shown in Fig. 3.2.

The semicanonical KS HOMO-LUMO gap for the C_6H_6 system is 5.13 eV whereas for LiNa it is 1.31 eV. Increasing the number of grid points from 25 to 200 for C_6H_6 results in a change in isotropic static polarizability (α_{iso}) of 0.24 a.u. whereas the same increase in the case of LiNa results in a change in α_{iso} of 34.01 a.u., as can be seen from Fig. 3.2. Systems with

small HOMO-LUMO gap would require a large number of frequency grid points to obtain converged static polarizabilities. Note that quadrature weight derivatives are not taken into account in this implementation.

3.3.3 Small molecules testset

To analyze the accuracy of the implemented GKS-spRPA static polarizabilities and compare it with other quantum chemical methods we gathered a set of 25 atoms and small molecules. The geometries of these molecules were optimized at the MP2/cc-pVTZ level wherever experimental geometries [195] were not available. A comparison of the GKS-spRPA method with HF, MP2, PBE and PBE0 is presented in Fig. 3.3 followed by a statistical analysis of the errors in Table 3.1. All the analytical polarizabilities within GKS-spRPA were calculated with the def2-QZVPPD basis set with PBE semilocal input and 100 frequency grid points. The reference CCSD(T) polarizabilities were calculated numerically using the def2-QZVPPD basis set or are obtained from the numerical CCSD(T) results of Hait et al. [196] or the analytical CCSD-F12 calculations of Bokhan et al. [197].

The beryllium dimer is a difficult system for standard quantum chemical methods to treat accurately because of the necessity to not only describe long-range dispersion interactions but also static correlation due to the near-degeneracy between the low-lying excited states. [142] We had previously shown that the ground state potential energy surface of this system is much more accurately described by GKS-spRPA compared to post-KS RPA, optimized effective potential RPA (OEP-RPA) [70], MP2 and SL DFAs. [180] The %RD of the GKS-spRPA polarizabilities from the reference CCSD(T) for Be_2 is found to be 9% while for HF it is 42%. PBE, PBE0 and MP2 have %RDs of 22%, 26%, 27%, respectively. This shows that the accurate description of the energetics of the Be_2 at the equilibrium bond distance by GKS-spRPA is also replicated for static polarizabilities.

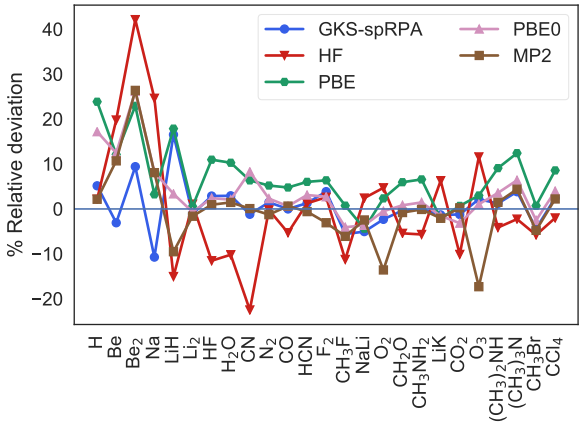

Figure 3.3: Isotropic static polarizabilities of several small molecules computed using GKS-spRPA is compared with HF, PBE, PBE0 and MP2 methods using the def2-QZVPPD basis set for all of the systems and methods.

The error analysis in Table 3.1 shows that the MAEs are the smallest for GKS-spRPA, followed by MP2, PBE0, PBE and HF. GKS-spRPA includes exact exchange at first order and correlation of the ring type to infinite order [22]. These particle-hole excitations are important to describe the polarization of electronic density and that is part of the reason for GKS-spRPA being successful in predicting static polarizabilities of these systems. While MP2 also contains particle-hole excitations it only has them at second order and the higher order excitations can be very important.

Table 3.1: The mean signed error (MSE), mean absolute error (MAE), root mean square error (RMSE) standard deviation (Std. Dev.) and the maximum absolute error (Max AE) in atomic unit (a.u.) for the testset of 25 polarizabilities are reported for several different methods. All calculations used the def2-QZVPPD basis set for all the atoms and the GKS-spRPA used the PBE semilocal input.

	GKS-spRPA	HF	PBE	PBE0	MP2
MSE	-0.92	3.56	1.70	1.35	0.63
MAE	2.34	5.42	3.08	2.74	2.77
Std. Dev.	4.66	10.89	4.77	5.29	5.39
Max AE	17.59	40.43	17.91	20.42	20.59

3.3.4 Conjugated polymers

The failure of local and semilocal DFAs for estimating the polarizabilities and hyperpolarizabilities of conjugated molecules which results in catastrophic overpolarization with increasing conjugation length is well documented. [17, 153] This has been attributed to the absence of a field-induced counteracting term in the response part of the XC potential in (semi)local DFAs [198]. A solution to this problem that was conceived in semiconductor physics was the addition of polarization dependent terms to the XC potential, which leads to polarization dependent DFT (PDDFT) [199], but the PDDFT XC kernels are unknown and the method has been applied usually for semiconductors where the susceptibility is overestimated by $\sim$ 10%, whereas for conjugated polymers the polarizability overestimations can be much larger. [153]

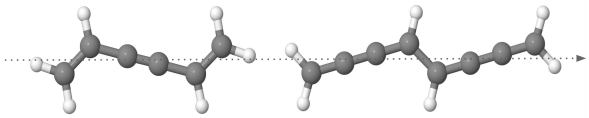

Figure 3.4: Structures of the polydiacetylene oligomer (PDA1, left) and polybutatriene oligomer (PBT2, right) as well as the longitudinal axis along which the calculated polarizabilities are reported in this study.

Yang and coworkers [159, 200] used the OEP exchange functional (OEP-EXX) [201] for calculating polarizabilities of conjugated oligomers and observed that their results were in good agreement with HF results. They concluded that the OEP-EXX procedure includes "ultra-nonlocal" exchange effects that are missing in (semi)local DFAs, but OEP-EXX still misses significant contributions from nonlocal long-range correlations. Nénon et al. [155] investigated the accuracy of tuned RSHs for calculating static polarizabilities of polydiacetylene (PDA) and polybutatriene (PBT) oligomers and concluded that the RSH functionals with larger tuning parameter performed better than the ones with smaller tuning parameter. Oviedo et al. [156] also performed tuned RSH calculations on PDA and PBT oligomers and found that with very large tuning parameters broken-symmetry solutions for PBT oligomers

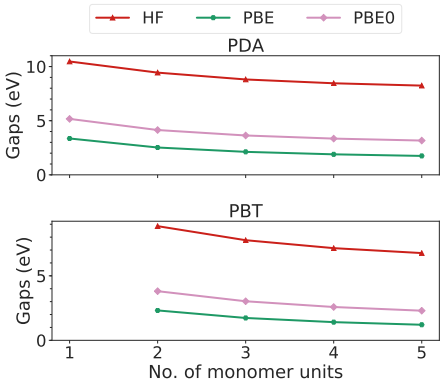

Figure 3.5: KS semilocal (PBE, PBE0) and HF HOMO-LUMO gaps (denoted as Gaps in the figure) in units of eV as a function of the number of monomer units of the PDA and PBT oligomers.

are obtained, which result in more accurate polarizabilities than the closed-shell singlet solutions that they obtain with smaller tuning parameters.

For these systems, the semilocal density functional approximations result in increasingly smaller HOMO-LUMO gaps as the system size increases which is depicted in Fig. 3.5. As the gap gets closer to zero, the static polarizability starts to become divergent for (semi)local DFAs.

We have used the GKS-spRPA method to calculate analytical polarizabilities of these polymers, the resulting %RDs with respect to the reference CCSD(T)-F12 calculations [156] are reported in Fig. 3.6. The GKS-spRPA results were obtained with a semilocal PBE input, def2-TZVPPD basis set, DFT numerical integration grids of size 4 [202] and 60 frequency grid points. The PBE and HF calculations were also carried out with the def2-TZVPPD basis set and numerical integration grids of size 4 was used for the PBE calculations. The CAM-B3LYP results, the reference CCSD(T)-F12 results as well as the optimized geometries of all the molecules were obtained from Oviedo et al. [156], who used the cc-PVDZ basis

set, froze the core electrons and performed three-point numerical finite field calculations to obtain the numerical CCSD(T)-F12 static polarizabilities.

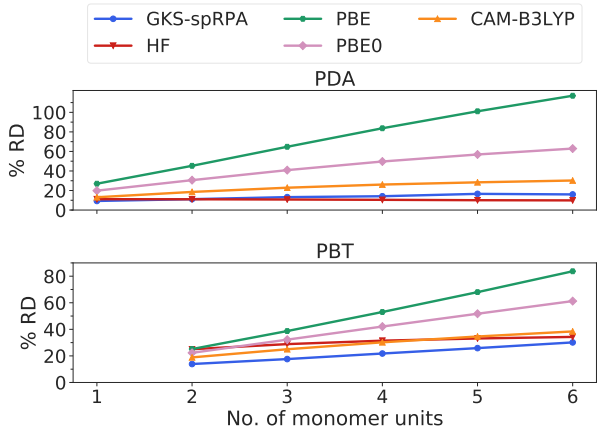

Figure 3.6: %RD in the longitudinal static polarizabilities as a function of the number of monomer units of the PDA (up) and PBT (down) oligomers calculated using GKS-spRPA with the def2-TZVPPD basis set and PBE semilocal input, compared to the HF, PBE and CAM-B3LYP methods.

As displayed in Fig. 3.6, the errors in static polarizabilities rapidly increase with the system size for the PBE functional. In case of PDA5, the PBE results reach a %RD of $\geq 100\%$. The GKS-spRPA errors, on the other hand are almost independent of the system size for the PDA oligomers with a mean %RD of 13% while HF, PBE, PBE0 and CAM-B3LYP result in mean %RDs of 11%, 73%, 43% and 23%, respectively. For the PBT oligomers, the mean %RD for GKS-spRPA, HF, PBE, PBE0 and CAM-B3LYP are 22%, 31%, 54%, 42% and 29%, respectively. The GKS-spRPA static polarizabilities for both the PDA and PBT oligomers are more accurate than the CAM-B3LYP results suggesting that the combination of exact HF exchange and long-range correlations contained in the GKS-spRPA functional are responsible for its better performance. However, the GKS-spRPA is not a functional self-consistent scheme which means that it has some dependence on the input semilocal DFA through the semicanonical projected semilocal orbital energies (for example in Eq. 3.9). This remaining undesirable dependence on the (semi)local KS input could be responsible for

the observed errors. The self-correlation error present in the GKS-spRPA energy functional also contributes to the errors in polarizabilities which can be partially corrected by including beyond-RPA methods such as the AXK [42] and the SOSEX [41].

3.3.5 Static polarizabilities of metallocenes

Transition metal metallocenes (TMM) exhibit diverse electronic structures with partially occupied d orbitals and multiple low lying spin configurations. These properties make them ideal building blocks for molecular spintronic [203] and optoelectronic [204] devices. Theoretical predictions polarizabilities and hyperpolarizabilities of TMMs would help in designing and tuning the properties of these advanced devices. However, TMMs pose challenges to conventional quantum chemical methods because of the small HOMO-LUMO gap due to several low lying spin configurations. Experimental polarizabilities of the d^6 metallocenes namely ferrocene, ruthenocene and osmocene were obtained using gas phase refractivity measurements by Hohm et al. [182, 205]. We tested the accuracy of our GKS-spRPA method

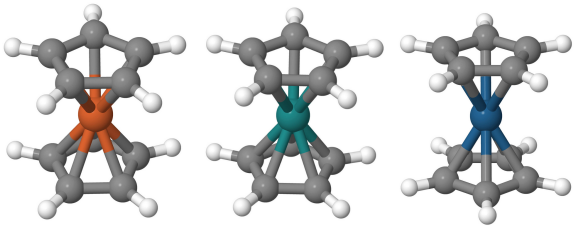

Figure 3.7: Structures of ferrocene ($Fe(C_5H_5)_2$), ruthenocene ($Ru(C_5H_5)_2$) and osmocene ($Os(C_5H_5)_2$) (left to right).

for these metallocenes for which the structures were obtained from Pansini et al. [206]. The ground state minimum energy structures of the Fe, Ru and Os metallocenes have D_3, C_2 and C_i symmetries, respectively as shown in Fig. 3.7. The ground spin states of all these compounds were found to be singlet. GKS-spRPA polarizabilities were calculated using the PBE input, def2-TZVPPD basis set with DFT integration grid of size 4 [202] and using 60 frequency grid points.

Table 3.2: The mean signed error (MSE), mean absolute error (MAE), root mean square error (RMSE) and the maximum error (Max AE) in atomic unit (a.u.) for ferrocene, osmocene and ruthenocene. All calculations used the def2-QZVPPD basis set for all the atoms and the GKS-spRPA used the PBE semilocal input.

	GKS-spRPA	HF	PBE	PBE0	MP2
MSE	-1.87	-14.05	2.07	-3.69	0.86
MAE	2.02	14.05	2.07	3.69	1.54
RMSE	2.43	14.18	2.60	3.74	1.73
Max E	-3.50	-12.12	4.20	-3.23	2.64

It can be seen from Table 3.2 that the GKS-spRPA results are very accurate compared to the experimental results with a MAE of 2.02 a.u. which is similar to the MAEs using MP2 and PBE which are 1.54 and 2.07 a.u.. PBE0 worsens the results of PBE by predicting polarizabilities that are too small with a MAE of 3.69 *a.u.* whereas HF predicts the least accurate polarizabilities for these TMMs with a MAE of 14.05 a.u.

3.3.6 Static polarizabilities of sodium clusters

Experimental static polarizabilities of alkali metal clusters such as sodium and lithium clusters are known to have large uncertainties and poor reproducibility. [207, 208] For example from Na_6 to Na_7 the isotropic static polarizability (α_{iso}) according to Rayane et al.[207], decreases from 816.62 to 800.69, whereas there is an increase observed by Knight et al.[208], from 754.42 to 808.34. Both Knight et al., and Rayane et al. used molecular beam deflection of the Na_n clusters through a static inhomogeneous transverse electric field to measure the α_{iso} of the Na_n clusters. Accurate theoretical calculations of polarizabilities of these systems could resolve the uncertain experimental results.

Previous theoretical studies based on MP2 by Chandrakumar et al.[181], also suggest a decrease in the α_{iso} going from Na_6 to Na_7, while HF suggests an increase. These clusters are difficult systems because they can have multiple nearly degenerate local minimum energy

structures in the ground state. Furthermore clusters with odd number of electrons can have multiple nearly degenerate spin states that further complicate the electronic structure. Therefore, accurate theoretical benchmark calculations taking into account the fluxional nature of the metal cluster structures are necessary especially since these experiments are typically done at finite temperatures.

In this study, the GKS-spRPA α_{iso} are benchmarked for small Na_n clusters ($n = 2, 3, \ldots, 10$) and we aim to answer two questions: can GKS-spRPA predict the experimental results accurately?, and how important are the thermal contributions to α_{iso}? To answer the first question, the geometries of the Na_n clusters are optimized to acquire local minimum energy structures and then α_{iso} are calculated at these geometries to obtain the zero temperature results. To address the second question, ab initio molecular dynamics (AIMD) calculations are performed to simulate the equilibrium dynamics of the Na_n clusters, and using these MD trajectories 50 snapshots are randomly selected from which the trajectory averaged polarizabilities ($\bar{\alpha}_{iso}$) are calculated.

The geometries of the Na_n clusters were optimized within DFT using the B3-LYP functional and the def2-TZVPP basis set for the Na atom, gridsize 4 was used along with weight derivatives to obtain the local minimum energy structures of these clusters and the structures are shown in Fig. 3.8. The α_{iso} corresponding to these structures are reported in Table 3.3 for HF, PBE and GKS-spRPA methods and it can be seen that the deviations with respect to available experimental results can be large. The AIMD simulations were carried out using the B3-LYP functional and the def2-TZVPP basis set. A microcanonical ensemble was used for the simulation of ground state equilibrium dynamics ensuring conservation of energy. The AIMD simulations were run for a total of 10 ps with a 20 a.u. timestep. The first 1 *ps* of the trajectory was not used for sampling to allow the system to attain equilibrium and from the remaining 9 ps 50 snapshots were selected at random and used for the calculation of $\bar{\alpha}_{iso}$.

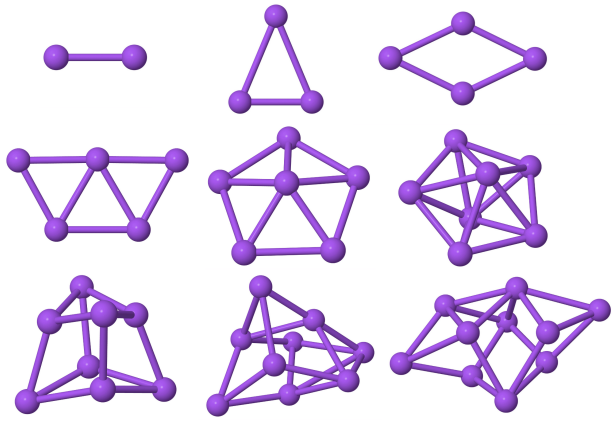

Figure 3.8: Structures of sodium clusters optimized with the B3-LYP[209] DFA using the def2-TZVPP basis set. Normal mode analysis is performed to confirm that these are local minimum energy structures.

Table 3.3: Calculated α_{iso} and $\bar{\alpha}_{iso}$ of Na_n clusters using GKS-spRPA, PBE and HF methods in a.u., compared to the experimental results.

	HF		PBE		GKS-spRPA		Expt.	
	α_{iso}	$\bar{\alpha}_{iso}$	α_{iso}	$\bar{\alpha}_{iso}$	α_{iso}	$\bar{\alpha}_{iso}$	Knight et al	Rayane et al.
Na_2	280.53		246.46		249.58		265.24	251.90
Na_3	463.99	618.55	434.03	436.80	416.87	415.91	444.83	464.70
Na_4	538.74	584.30	500.61	532.64	482.66	535.36	565.58	538.62
Na_5	648.28	690.67	621.40	623.87	612.26	621.25	630.03	710.92
Na_6	736.75	755.27	669.12	686.30	675.19	692.27	754.42	816.62
Na_7	768.02	900.12	706.82	710.88	714.56	724.10	808.34	800.69
Na_8	886.41	871.30	817.60	776.39	830.53	805.17	901.14	868.75
Na_9	1209.60	1108.76	974.90	982.07	977.24	988.28	1062.98	1042.49
Na_{10}	1100.08	1160.38	1020.34	1075.37	1029.24	1087.50	1309.33	1274.14

Fig. 3.9 depicts the calculated α_{iso} for the Na_n clusters using the 50 snapshots selected from the AIMD simulations for the GKS-spRPA, PBE and HF methods in the form of box plots. It can be observed that the spread in the HF α_{iso} is considerably larger for clusters with odd number of electrons which have an open shell electronic structure. Some of the Na_3 snapshots resulted in HF α_{iso} of ~ 900 $a.u.$ which is qualitatively wrong compared to the experimental results which are ≤ 500 a. u. for the Na_3 cluster. The spread in the GKS-spRPA results are fairly independent of whether the cluster has odd or even number of Na atoms and none of the snapshots result in qualitatively wrong over estimations of α_{iso} as is the case with HF.

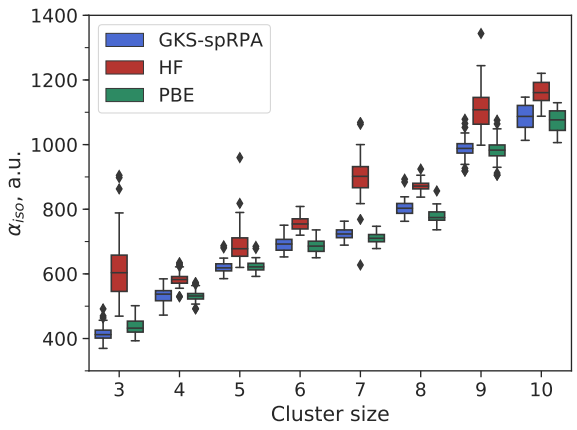

Figure 3.9: The calculated α_{iso} using GKS-spRPA, PBE and HF methods in a.u. for the 50 snapshots from the AIMD simulations are represented as box plots. The box represents the interquartile range (IQR) which is from the 25^{th} (first quartile, Q1) to the 75^{th} (third quartile, Q3) percentile of the data and the line inside the box represents the median. The whiskers denote Q1$-1.5\times$IQR and Q3$+1.5\times$IQR and data points that lie outside this range is denoted by solid black diamonds.

The mean absolute deviation (MAD) of the GKS-spRPA α_{iso} and $\bar{\alpha}_{iso}$ compared to the experimental results of Rayane et al., and Knight et al. are 95 and 78 a.u., respectively. The calculated $\bar{\alpha}_{iso}$ are closer to the experimental results by 17 a.u. compared to the α_{iso} for the GKS-spRPA method. The MAD of the HF α_{iso} and $\bar{\alpha}_{iso}$ are 64 and 71 a.u., respectively and the same for PBE the MADs are calculated respectively to be 94 and 84 a.u. This indicates thermal corrections of 7 a.u. and 10 a.u. for the Na_n clusters using the HF and PBE methods respectively.

Using these results it is concluded that the GKS-spRPA does not provide significantly better α_{iso} for the Na_n clusters compared to the HF and PBE methods. The maximum average thermal correction of 17 a.u. obtained using the GKS-spRPA method does not provide any conclusive evidence that thermal effects play an important role in determining the α_{iso} of the Na_n clusters.

3.4 Conclusions

The GKS-spRPA $\boldsymbol{\alpha}(0)$ within the RI approximation can be implemented with a computational scaling of only $\mathcal{O}(N^4 \log N)$ and storage of $\mathcal{O}(N^3)$ intermediates. Property optimized basis sets developed for getting converged time-dependent HF and KS polarizabilities and excitation energies also result in converged $\boldsymbol{\alpha}(0)$ for the GKS-spRPA functional with %RD of $\leq 1\%$ obtained using the def2-TZVPPD and QZVPPD basis sets. For small molecules, the GKS-spRPA results in more accurate $\boldsymbol{\alpha}(0)$ compared to HF, MP2, PBE and PBE0 while using the CCSD(T) method as the reference. PDA and PBT $\pi-$conjugated oligomers act as a stringent test for the accuracy of $\boldsymbol{\alpha}(0)$ predicted by DFAs and GKS-spRPA results have smaller %RD compared to the reference CCSD(T)-F12 results than PBE, PBE0, CAM-B3LYP and HF for these systems. These results show that the GKS-spRPA effectively addresses the problem of overpolarization that is encountered while using SL/hybrid DFAs for these systems and it provides more accurate results than the RSH functional CAM-B3LYP. The smaller errors obtained using GKS-spRPA, compared to SL, hybrid and RSH functionals can be attributed to the inclusion of exact HF exchange and long-range correlations, of which the latter is missing in RSHs. For the Na_n clusters the GKS-spRPA α_{iso} and the AIMD trajectory averaged $\bar{\alpha}_{iso}$ were found to qualitatively agree with the experiments and showed a monotonic increase with cluster size. Thermal averaging improved the results by 17 a.u. using the GKS-spRPA method which indicates that thermal effects are not very important for the α_{iso} of the Na_n clusters.

The errors in the GKS-spRPA method could be resulting from the fact that it still contains spurious self-correlation and that it is not a functional self-consistent scheme that still depends on the (semi)local KS potential. The first issue can be addressed using beyond-RPA methods such as the AXK [42] and SOSEX [41] while the second issue requires the development of functional self-consistent DFAs that would get rid of all the dependence on the semilocal KS input.

Chapter 4

Conclusions

This thesis presented the development and implementation of a generalized Kohn–Sham (GKS) scheme for the post-KS random phase approximation (RPA) method, called the GKS semicanonical projected RPA (GKS-spRPA). Orbital self-consistent schemes developed for explicitly potential dependent energy functionals, such as the optimized effective potential (OEP) method result in two different densities; one that is obtained from the orbitals and the other, presumably more accurate, that is obtained from the Hellmann-Feynman theorem. The functional self-consistency (FSC) condition states that a uniquely determined KS potential stationarize the energy functional that is explicitly dependent on it. Imposing the functional self-consistency condition would result in an energy functional whose KS density and the Hellmann-Feynman density will be identical. The GKS-spRPA functional approximately satisfies the FSC condition by requiring that the GKS potential defining the energy and the potential that is obtained as its functional derivative have the same ground state density matrix.

The density-driven errors suffered by the semilocal (SL) density functional approximations (DFAs) as well as by post-KS RPA are cured by using the orbital self-consistent GKS-

spRPA method. The GKS-spRPA significantly improves the description of noncovalent interactions, while covalent binding energies are slightly improved compared to the post-KS RPA. Approximate ionization potentials (IPs) and electron affinities (EAs) are obtained from the eigenvalues of the GKS-spRPA one-particle Hamiltonian. The GKS-spRPA IPs match the experimental IPs of atoms and molecules with the precision of a few tenths of an eV which is more accurate than commonly used G_0W_0, which is a Greens function theory (GFT) based method. The calculations of approximate quasiparticle energies as well as ground state energies using the same Lagrangian framework is possible within the GKS-spRPA whereas this is not a feature of other methods such as SL DFAs, GW and correlated wave function based methods such as Møller-Plesset (MP) perturbation theory.

Furthermore, static polarizabilities ($\boldsymbol{\alpha}(0)$) within the GKS-spRPA were developed within the Lagrangian framework and implemented at a computational cost of $\mathcal{O}(N^4 \log(N))$ which is on the same order of that of a GKS-spRPA geometrical gradients calculation. $\boldsymbol{\alpha}(0)$ based on the GKS-spRPA is more accurate than SL, hybrid and range-separated hybrid (RSH) DFAs for $\pi-$conjugated polymers such as polydiacetylene (PDA) and polybutatriene (PBT). SL DFAs suffer from the problem of overpolarization for these $\pi-$conjugated systems and result in catastrophic overestimation of polarizabilities. GKS-spRPA functional contains nonlocal HF exchange as well as nonlocal correlation that helps it counter the errors made by SL functionals as well as by RSH DFAs which typically contain only nonlocal exchange.

Through efficient implementation and careful analysis of the results, the conclusion of this thesis is that the GKS-spRPA is a method which shares favorable characteristics of both DFT and GFT and is accurate, efficient and universally applicable for calculations of energies, geometries, dipole moments, IPs, EAs and static polarizabilities.

Bibliography

[1] J. Hollas, *Modern spectroscopy* (Wiley, 2004).

[2] S. Mukamel, *Principles of nonlinear optical spectroscopy*, Oxford series in optical and imaging sciences (Oxford University Press, 1995).

[3] P. Hohenberg and W. Kohn, "Inhomogeneous electron gas", Phys. Rev. **136**, 864 (1964).

[4] K. Burke, "Perspective on density functional theory", J. Chem. Phys. **136**, 150901 (2012).

[5] W. Kohn and L. J. Sham, "Self-consistent equations including exchange and correlation effects", Phys. Rev. **140**, A1133 (1965).

[6] S. H. Vosko, L. Wilk, and M. Nusair, "Accurate spin-dependent electron liquid correlation energies for local spin density calculations: a critical analysis", Can. J. Phys. **58**, 1200 (1980).

[7] J. P. Perdew, K. Burke, and M. Ernzerhof, "Generalized gradient approximation made simple", Phys. Rev. Lett. **77**, 3865 (1996).

[8] J. Tao, J. P. Perdew, V. N. Staroverov, and G. E. Scuseria, "Climbing the Density Functional Ladder: Nonempirical Meta–Generalized Gradient Approximation Designed for Molecules and Solids", Phys. Rev. Lett. **91**, 146401 (2003).

[9] J. P. Perdew, M. Ernzerhof, and K. Burke, "Rationale for mixing exact exchange with density functional approximations", J. Chem. Phys. **105**, 9982 (1996).

[10] A. D. Becke, "A new mixing of Hartree–Fock and local density-functional theories", J. Chem. Phys. **98**, 1372 (1993).

[11] D. Rappoport, N. R. M. Crawford, F. Furche, and K. Burke, "Approximate Density Functionals: Which Should I Choose?", in *Encyclopedia of inorganic chemistry* (American Cancer Society, 2009), pp. 159–172.

[12] A. Tajti, P. G. Szalay, A. G. Császár, M. Kállay, J. Gauss, E. F. Valeev, B. A. Flowers, J. Vázquez, and J. F. Stanton, "HEAT: High accuracy extrapolated ab initio thermochemistry", J. Chem. Phys. **121**, 11599 (2004).

[13] L. Goerigk and S. Grimme, "A thorough benchmark of density functional methods for general main group thermochemistry, kinetics, and noncovalent interactions", Phys. Chem. Chem. Phys. **13**, 6670 (2011).

[14] J. P. Perdew and A. Zunger, "Self-interaction correction to density-functional approximations for many-electron systems", Phys. Rev. B **23**, 5048 (1981).

[15] E. R. Johnson, I. D. Mackie, and G. A. DiLabio, "Dispersion interactions in density-functional theory", J. Phys. Org. Chem. **22**, 1127 (2009).

[16] D. Lee, F. Furche, and K. Burke, "Accuracy of electron affinities of atoms in approximate density functional theory", J. Phys. Chem. Lett. **1**, 2124 (2010).

[17] B. Champagne, E. A. Perpéte, D. Jacquemin, S. J. A. van Gisbergen, E.-J. Baerends, C. Soubra-Ghaoui, K. A. Robins, and B. Kirtman, "Assessment of Conventional Density Functional Schemes for Computing the Dipole Moment and (Hyper)polarizabilities of Push Pull π Conjugated Systems", J. Phys. Chem. A **104**, 4755 (2000).

[18] J. Sun, A. Ruzsinszky, and J. P. Perdew, "Strongly constrained and appropriately normed semilocal density functional", Phys. Rev. Lett. **115**, 036402 (2015).

[19] F. Furche and T. Van Voorhis, "Fluctuation-dissipation theorem density-functional theory", J. Chem. Phys. **122**, 164106 (2005).

[20] D. Bohm and D. Pines, "A Collective Description of Electron Interactions. I. Magnetic Interactions", Phys. Rev. **82**, 625 (1951).

[21] D. Pines and D. Bohm, "A Collective Description of Electron Interactions: II. Collective vs Individual Particle Aspects of the Interactions", Phys. Rev. **85**, 338 (1952).

[22] M. Gell-Mann and K. A. Brueckner, "Correlation energy of an electron gas at high density", Phys. Rev. **106**, 364 (1957).

[23] A. D. McLachlan and M. A. Ball, "Time-Dependent Hartree—Fock Theory for Molecules", Rev. Mod. Phys. **36**, 844 (1964).

[24] D. J. Rowe, "Equations-of-Motion Method and the Extended Shell Model", Rev. Mod. Phys. **40**, 153 (1968).

[25] T.-I. Shibuya and V. McKoy, "Higher random-phase approximation as an approximation to the equations of motion", Phys. Rev. A **2**, 2208 (1970).

[26] E. S. Nielsen, P. Jørgensen, and J. Oddershede, "Transition moments and dynamic polarizabilities in a second order polarization propagator approach", J. Chem. Phys. **73**, 6238 (1980).

[27] J. Oddershede, P. Jørgensen, and D. L. Yeager, "Polarization propagator methods in atomic and molecular calculations", Comput. Phys. Rep. **2**, 33 (1984).

[28] D. C. Langreth and J. P. Perdew, "Exchange-correlation energy of a metallic surface: Wave-vector analysis", Phys. Rev. B **15**, 2884 (1977).

[29] O. Gunnarsson and B. I. Lundqvist, "Exchange and correlation in atoms, molecules, and solids by spin-density functional formalism", Phys. Rev. B **13**, 4274 (1976).

[30] J. F. Dobson and J. Wang, "Successful Test of a Seamless van der Waals Density Functional", Phys. Rev. Lett. **82**, 2123 (1999).

[31] F. Furche, "Molecular tests of the random phase approximation to the exchange-correlation energy functional", Phys. Rev. B **64**, 195120 (2001).

[32] A. Heßelmann and A. Görling, "Random-phase approximation correlation methods for molecules and solids", Mol. Phys. **109**, 2473 (2011).

[33] X. Ren, P. Rinke, C. Joas, and M. Scheffler, "Random-phase approximation and its applications in computational chemistry and materials science", J. Mater. Sci. **47**, 7447 (2012).

[34] G. P. Chen, V. K. Voora, M. M. Agee, S. G. Balasubramani, and F. Furche, "Random-phase approximation methods", Annu. Rev. Phys. Chem. **68**, 421 (2017).

[35] H. Eshuis, J. Yarkony, and F. Furche, "Fast computation of molecular random phase approximation correlation energies using resolution of the identity and imaginary frequency integration", J. Chem. Phys. **132**, 234114 (2010).

[36] C. Møller and M. S. Plesset, "Note on an approximation treatment for many-electron systems", Phys. Rev. **46**, 618 (1934).

[37] M. Häser, "Møller-Plesset (MP2) perturbation theory for large molecules", Theoret. Chim. Acta. **87**, 147 (1993).

[38] S. Kurth and J. P. Perdew, "Density-functional correction of random-phase-approximation correlation with results for jellium surface energies", Phys. Rev. B **59**, 10461 (1999).

[39] Z. Yan, J. P. Perdew, and S. Kurth, "Density functional for short-range correlation: Accuracy of the random-phase approximation for isoelectronic energy changes", Phys. Rev. B **61**, 16430 (2000).

[40] D. L. Freeman, "Coupled-cluster expansion applied to the electron gas: Inclusion of ring and exchange effects", Phys. Rev. B **15**, 5512 (1977).

[41] A. Grüneis, M. Marsman, J. Harl, L. Schimka, and G. Kresse, "Making the random phase approximation to electronic correlation accurate", J. Chem. Phys. **131**, 154115 (2009).

[42] J. E. Bates and F. Furche, "Communication: random phase approximation renormalized many-body perturbation theory", J. Chem. Phys. **139**, 171103 (2013).

[43] A. M. Burow, J. E. Bates, F. Furche, and H. Eshuis, "Analytical First-Order Molecular Properties and Forces within the Adiabatic Connection Random Phase Approximation", J. Chem. Theory Comput. **10**, 180 (2014).

[44] P. Pulay, "Analytical derivative methods in quantum chemistry", in *Advances in chemical physics*, Vol. 69, edited by K. P. Lawley, I. Prigogine, and S. A. Rice (John Wiley & Sons, 2007), pp. 241–286.

[45] J. F. Stanton and J. Gauss, "Analytic second derivatives in high-order many-body perturbation and coupled-cluster theories: computational considerations and applications", Int. Rev. Phys. Chem. **19**, 61 (2000).

[46] P. Jørgensen and T. Helgaker, "Møller–Plesset energy derivatives", J. Chem. Phys. **89**, 1560 (1988).

[47] T. Helgaker, P. Jørgensen, and N. C. Handy, "A numerically stable procedure for calculating Møller-Plesset energy derivatives, derived using the theory of Lagrangians", Theor. chem. Acc. **76**, 227 (1989).

[48] J. A. Pople, R. Krishnan, H. B. Schlegel, and J. S. Binkley, "Derivative studies in Hartree-Fock and Møller-Plesset theories", Int. J. Quantum Chem. **16**, 225 (1979).

[49] M. Fuchs, Y.-M. Niquet, X. Gonze, and K. Burke, "Describing static correlation in bond dissociation by Kohn-Sham density functional theory", J. Chem. Phys. **122**, 094116 (2005).

[50] T. M. Henderson and G. E. Scuseria, "The connection between self-interaction and static correlation: a random phase approximation perspective", Mol. Phys. **108**, 2511 (2010).

[51] P. Deglmann, F. Furche, and R. Ahlrichs, "An efficient implementation of second analytical derivatives for density functional methods", Chem. Phys. Lett. **362**, 511 (2002).

[52] F. Furche, B. T. Krull, B. D. Nguyen, and J. Kwon, "Accelerating molecular property calculations with nonorthonormal Krylov space methods", J. Chem. Phys. **144**, 174105 (2016).

[53] J. Rekkedal, S. Coriani, M. F. Iozzi, A. M. Teale, T. Helgaker, and T. B. Pedersen, "Communication: analytic gradients in the random-phase approximation", J. Chem. Phys. **139**, 081101 (2013).

[54] B. Mussard, P. G. Szalay, and J. G. Ángyán, "Analytical Energy Gradients in Range-Separated Hybrid Density Functional Theory with Random Phase Approximation", J. Chem. Theory. Comput. **10**, 1968 (2014).

[55] H. Fukutome, "Unrestricted Hartree-Fock theory and its applications to molecules and chemical reactions", Int. J. Quantum Chem. **20**, 955 (1981).

[56] D. J. Thouless, *The quantum mechanics of many-body systems: second edition*, Dover Books on Physics (Dover Publications, 2013).

[57] J. F. Stanton and J. Gauss, "A discussion of some problems associated with the quantum mechanical treatment of open-shell molecules", in *Adv. chem. phys.* Vol. 125, edited by S. A. Rice and I. Prigogine (John Wiley & Sons, Inc., 2003), pp. 101–146.

[58] T. H. Dunning, "Gaussian basis sets for use in correlated molecular calculations. I. The atoms boron through neon and hydrogen", J. Chem. Phys. **90**, 1007 (1989).

[59] K. Huber, *Molecular Spectra and Molecular Structure: IV. Constants of Diatomic Molecules* (Springer US, 2013).

[60] G. Graner and K. Kuchitsu, *Structure data of free polyatomic molecules*, Landolt-Börnstein: Molecules and radicals (Springer Berlin Heidelberg, 2001).

[61] M. D. Harmony, V. W. Laurie, R. L. Kuczkowski, R. H. Schwendeman, D. A. Ramsay, F. J. Lovas, W. J. Lafferty, and A. G. Maki, "Molecular structures of gas-phase polyatomic molecules determined by spectroscopic methods", J. Phys. Chem. Ref. Data **8**, 619 (1979).

[62] R. P. Tuckett, A. R. Dale, D. M. Jaffey, P. S. Jarrett, and T. Kelly, "The A $^2\Pi_u \rightarrow$ X $^2\Pi_g$ electronic emission spectrum of the fluorine molecular ion F_2^+ studied in a supersonic beam", Molec. Phys. **49**, 475 (1983).

[63] H. Eshuis, J. E. Bates, and F. Furche, "Electron correlation methods based on the random phase approximation", Theor. Chem. Acc. **131**, 1084 (2012).

[64] J. F. Dobson and T. Gould, "Calculation of dispersion energies", J. Phys. Condens. Matter **24**, 073201 (2012).

[65] S. Lebègue, J. Harl, T. Gould, J. G. Ángyán, G. Kresse, and J. F. Dobson, "Cohesive properties and asymptotics of the dispersion interaction in graphite by the random phase approximation", Phys. Rev. Lett. **105**, 196401 (2010).

[66] M.-C. Kim, E. Sim, and K. Burke, "Understanding and reducing errors in density functional calculations", Phys. Rev. Lett. **111**, 073003 (2013).

[67] A. Wasserman, J. Nafziger, K. Jiang, M.-C. Kim, E. Sim, and K. Burke, "The importance of being inconsistent", Ann. Rev. Phys. Chem. **68**, 555 (2017).

[68] A. J. Cohen, P. Mori-Sanchez, and W. Yang, "Insights into current limitations of density functional theory", Science **321**, 792 (2008).

[69] M. Hellgren, F. Caruso, D. R. Rohr, X. Ren, A. Rubio, M. Scheffler, and P. Rinke, "Static correlation and electron localization in molecular dimers from the self-consistent RPA and GW approximation", Phys. Rev. B **91**, 165110 (2015).

[70] N. L. Nguyen, N. Colonna, and S. de Gironcoli, "Ab initio self-consistent total-energy calculations within the EXX/RPA formalism", Phys. Rev. B **90**, 045138 (2014).

[71] P. Bleiziffer, A. Heßelmann, and A. Görling, "Efficient self-consistent treatment of electron correlation within the random phase approximation", J. Chem. Phys. **139**, 084113 (2013).

[72] P. Verma and R. J. Bartlett, "Increasing the applicability of density functional theory. II. Correlation potentials from the random phase approximation and beyond", J. Chem. Phys. **136**, 044105 (2012).

[73] M. Hellgren and U. von Barth, "Correlation Potential in Density Functional Theory at the GW Level: Spherical Atoms", Phys. Rev. B **76**, 075107 (2007).

[74] Y. Jin, D. Zhang, Z. Chen, N. Q. Su, and W. Yang, "Generalized optimized effective potential for orbital functionals and self-consistent calculation of random phase approximations", J. Phys. Chem. Lett. **8**, 4746 (2017).

[75] R. W. Godby, M. Schlüter, and L. J. Sham, "Self-energy operators and exchange-correlation potentials in semiconductors", Phys. Rev. B **37**, 10159 (1988).

[76] M. S. Hybertsen and S. G. Louie, "Electron correlation in semiconductors and insulators: Band gaps and quasiparticle energies", Phys. Rev. B **34**, 5390 (1986).

[77] G. Onida, L. Reining, and A. Rubio, "Electronic excitations: density-functional versus many-body Green's-function approaches", Rev. Mod. Phys. **74**, 601 (2002).

[78] M. van Schilfgaarde, T. Kotani, and S. Faleev, "Quasiparticle self-consistent GW theory", Phys. Rev. Lett. **96**, 226402 (2006).

[79] F. Kaplan, M. E. Harding, C. Seiler, F. Weigend, F. Evers, and M. J. van Setten, "Quasi-Particle Self-Consistent GW for Molecules", J. Chem. Theory Comput. **12**, 2528 (2016).

[80] G. Borghi, A. Ferretti, N. L. Nguyen, I. Dabo, and N. Marzari, "Koopmans-compliant functionals and their performance against reference molecular data", Phys. Rev. B **90**, 075135 (2014).

[81] S. Refaely-Abramson, S. Sharifzadeh, N. Govind, J. Autschbach, J. B. Neaton, R. Baer, and L. Kronik, "Quasiparticle spectra from a nonempirical optimally tuned range-separated hybrid density functional", Phys. Rev. Lett. **109**, 226405 (2012).

[82] M. J. van Setten, F. Weigend, and F. Evers, "The GW-Method for Quantum Chemistry Applications: Theory and Implementation", J. Chem. Theory Comput. **9**, 232 (2013).

[83] B. Holm and U. von Barth, "Fully self-consistent GW self-energy of the electron gas", Phys. Rev. B **57**, 2108 (1998).

[84] A. Stan, N. E. Dahlen, and R. van Leeuwen, "Fully self-consistent GW calculations for atoms and molecules", Europhys. Lett. **76**, 298 (2006).

[85] F. Caruso, P. Rinke, X. Ren, A. Rubio, and M. Scheffler, "Self-consistent GW: All-electron implementation with localized basis functions", Phys. Rev. B **88**, 075105 (2013).

[86] A. Seidl, A. Görling, P. Vogl, J. A. Majewski, and M. Levy, "Generalized Kohn-Sham schemes and the band-gap problem", Phys. Rev. B **53**, 3764 (1996).

[87] X. Ren, P. Rinke, G. E. Scuseria, and M. Scheffler, "Renormalized second-order perturbation theory for the electron correlation energy: Concept, implementation, and benchmarks", Phys. Rev. B **88**, 035120 (2013).

[88] J. E. Moussa, "Cubic-scaling algorithm and self-consistent field for the random-phase approximation with second-order screened exchange", J. Chem. Phys. **140**, 014107 (2014).

[89] J. P. Perdew, W. Yang, K. Burke, Z. Yang, E. K. U. Gross, M. Scheffler, G. E. Scuseria, T. M. Henderson, I. Y. Zhang, A. Ruzsinszky, H. Peng, J. Sun, E. Trushin, and A. Görling, "Understanding band gaps of solids in generalized Kohn–Sham theory", Proc. Natl. Acad. Sci. **114**, 2801 (2017).

[90] V. N. Staroverov, G. E. Scuseria, and E. R. Davidson, "Optimized effective potentials yielding Hartree-Fock energies and densities", J. Chem. Phys. **124**, 141103 (2006).

[91] A. Heßelmann, A. W. Gotz, F. Della Sala, and A. Görling, "Numerically stable optimized effective potential method with balanced Gaussian basis sets", J. Chem. Phys. **127**, 054102 (2007).

[92] T. Heaton-Burgess, F. A. Bulat, and W. Yang, "Optimized effective potentials in finite basis sets", Phys. Rev. Lett. **98**, 256401 (2007).

[93] T. Heaton-Burgess and W. Yang, "Optimized effective potentials from arbitrary basis sets", J. Chem. Phys. **129**, 194102 (2008).

[94] A. Görling and M. Levy, "Exact Kohn-Sham scheme based on perturbation theory", Phys. Rev. A **50**, 196 (1994).

[95] A. Facco Bonetti, E. Engel, R. N. Schmid, and R. M. Dreizler, "Investigation of the correlation potential from Kohn-Sham perturbation theory", Phys. Rev. Lett. **86**, 2241 (2001).

[96] S. Ivanov, S. Hirata, I. Grabowski, and R. J. Bartlett, "Connections between second-order Görling-Levy and many-body perturbation approaches in density functional theory", J. Chem. Phys. **118**, 461 (2003).

[97] K. J. H. Giesbertz and E. J. Baerends, "Aufbau derived from a unified treatment of occupation numbers in Hartree–Fock, Kohn–Sham, and natural orbital theories with the Karush–Kuhn–Tucker conditions for the inequality constraints $n_i \leq 1$ and $n_i \geq 0$", J. Chem. Phys. **132**, 194108 (2010).

[98] P. R. T. Schipper, O. V. Gritsenko, and E. J. Baerends, "One-determinantal pure state versus ensemble Kohn-Sham solutions in the case of strong electron correlation: CH_2 and C_2", Theor. Chem. Acc. **99**, 329 (1998).

[99] J. E. Harriman, "Densities, operators, and basis sets", Phys. Rev. A **34**, 29 (1986).

[100] R. Cuevas-Saavedra, P. W. Ayers, and V. N. Staroverov, "Kohn-Sham exchange-correlation potentials from second-order reduced density matrices", J. Chem. Phys. **143**, 244116 (2015).

[101] E. H. Lieb, "Density functionals for Coulomb systems", Int. J. Quant. Chem. **24**, 243.

[102] W. Yang, P. W. Ayers, and Q. Wu, "Potential Functionals: Dual to Density Functionals and Solution to the v-Representability Problem", Phys. Rev. Lett. **92**, 146404 (2004).

[103] J. Talman and W. Shadwick, "Optimized effective atomic central potential", Phys. Rev. A **14**, 36 (1976).

[104] P. Bleiziffer, M. Krug, and A. Görling, "Self-consistent Kohn-Sham method based on the adiabatic-connection fluctuation-dissipation theorem and the exact-exchange kernel", J. Chem. Phys. **142**, 244108 (2015).

[105] P. W. Ayers and W. Yang, "Legendre-transform functionals for spin-density-functional theory", J. Chem. Phys. **124**, 224108 (2006).

[106] F. Tandetzky, J. K. Dewhurst, S. Sharma, and E. K. U. Gross, "Multiplicity of solutions to GW-type approximations", Phys. Rev. B **92**, 115125 (2015).

[107] M. Levy and J. P. Perdew, "The constrained search formulation of density functional theory", in *Density functional methods in physics*, edited by R. M. Dreizler and J. da Providência (Springer US, Boston, MA, 1985), pp. 11–30.

[108] D. Langreth and J. Perdew, "The exchange-correlation energy of a metallic surface", Solid State Commun. **17**, 1425 (1975).

[109] J. Toulouse, W. Zhu, J. G. Ángyán, and A. Savin, "Range-separated density-functional theory with the random-phase approximation: Detailed formalism and illustrative applications", Phys. Rev. A **82**, 032502 (2010).

[110] T. Gilbert, "Hohenberg-Kohn theorem for nonlocal external potentials", Phys. Rev. B **12**, 2111 (1975).

[111] K. Pernal, "Effective potential for natural spin orbitals", Phys. Rev. Lett. **94**, 233002 (2005).

[112] F. Aryasetiawan and O. Gunnarsson, "The GW method", Rep. Prog. Phys. **61**, 237 (1998).

[113] B. Ramberger, T. Schäfer, and G. Kresse, "Analytic interatomic forces in the random phase approximation", Phys. Rev. Lett. **118**, 106403 (2017).

[114] K. A. Peterson and C. Puzzarini, "Systematically convergent basis sets for transition metals. II. Pseudopotential-based correlation consistent basis sets for the group 11 (Cu, Ag, Au) and 12 (Zn, Cd, Hg) elements", Theor. Chem. Acc. **114**, 283 (2005).

[115] K. R. Lykke, K. K. Murray, and W. C. Lineberger, "Threshold photodetachment of H^-", Phys. Rev. A **43**, 6104 (1991).

[116] G. Haeffler, D. Hanstorp, I. Kiyan, A. E. Klinkmüller, U. Ljungblad, and D. J. Pegg, "Electron affinity of Li: A state-selective measurement", Phys. Rev. A **53**, 4127 (1996).

[117] C. Blondel, C. Delsart, and F. Goldfarb, "Electron spectrometry at the μ eV level and the electron affinities of Si and F", J. Phys. B **34**, L281 (2001).

[118] H. Hotop and W. C. Lineberger, "Dye-laser photodetachment studies of Au^-, Pt^-, PtN^-, and Ag^-", J. Chem. Phys. **58**, 2379 (1973).

[119] K. Krause, M. E. Harding, and W. Klopper, "Coupled-cluster reference values for the GW27 and GW100 test sets for the assessment of GW methods", Mol. Phys. **113**, 1952 (2015).

[120] F. Weigend and R. Ahlrichs, "Balanced basis sets of split valence, triple zeta valence and quadruple zeta valence quality for H to Rn: Design and assessment of accuracy", Phys. Chem. Chem. Phys. **7**, 3297 (2005).

[121] D. E. Woon and T. H. Dunning, "Gaussian basis sets for use in correlated molecular calculations. V. Core-valence basis sets for boron through neon", J. Chem. Phys. **103**, 4572 (1995).

[122] Y. M. Niquet and X. Gonze, "Band-gap energy in the random-phase approximation to density-functional theory", Phys. Rev. B **70**, 245115 (2004).

[123] P. Jurecka, J. Sponer, J. Cerny, and P. Hobza, "Benchmark database of accurate (MP2 and CCSD(T) complete basis set limit) interaction energies of small model complexes, DNA base pairs, and amino acid pairs", Phys. Chem. Chem. Phys. **8**, 1985 (2006).

[124] T. Takatani, E. G. Hohenstein, M. Malagoli, M. S. Marshall, and C. D. Sherrill, "Basis set consistent revision of the S22 test set of noncovalent interaction energies", J. Phys. Chem. **132**, 144104 (2010).

[125] K. A. Peterson and T. H. Dunning Jr., "Accurate correlation consistent basis sets for molecular core-valence correlation effects: The second row atoms Al-Ar, and the first row atoms B-Ne revisited", J. Chem. Phys. **117**, 10548 (2002).

[126] T. van Mourik and T. H. Dunning Jr., "A new ab initio potential energy curve for the helium dimer", J. Chem. Phys. **111**, 9248 (1999).

[127] R. Hellmann, E. Bich, and E. Vogel, "Ab initio potential energy curve for the neon atom pair and thermophysical properties of the dilute neon gas. I. Neon–neon interatomic potential and rovibrational spectra", Mol. Phys. **106**, 133 (2008).

[128] K. Patkowski, G. Murdachaew, C.-M. Fou, and K. Szalewicz, "Accurate ab initio potential for argon dimer including highly repulsive region", Mol. Phys. **103**, 2031 (2005).

[129] J. M. Waldrop, B. Song, K. Patkowski, and X. Wang, "Accurate ab initio potential for the krypton dimer and transport properties of the low-density krypton gas", J. Chem. Phys. **142**, 204307 (2015).

[130] A. K. Wilson, T. van Mourik, and T. H. Dunning Jr., "Gaussian basis sets for use in correlated molecular calculations. VI. Sextuple zeta correlation consistent basis sets for boron through neon", J. Mol. Struct. (THEOCHEM) **388**, 339 (1996).

[131] T. H. Dunning, K. A. Peterson, and A. K. Wilson, "Gaussian basis sets for use in correlated molecular calculations. X. The atoms aluminum through argon revisited", J. Chem. Phys. **114**, 9244 (2001).

[132] K. Raghavachari, G. W. Trucks, J. A. Pople, and M. Head-Gordon, "A 5^{th}-order perturbation comparison of electron correlation theories", Chem. Phys. Lett. **157**, 479 (1989).

[133] X. G. Ren, A. Tkatchenko, P. Rinke, and M. Scheffler, "Beyond the random-phase approximation for the electron correlation energy: the importance of single excitations", Phys. Rev. Lett. **106**, 153003 (2011).

[134] K. Patkowski, V. Špirko, and K. Szalewicz, "On the elusive twelfth vibrational state of beryllium dimer", Science **326**, 1382 (2009).

[135] D. Feller and K. A. Peterson, "Re-examination of atomization energies for the Gaussian-2 set of molecules", J. Chem. Phys. **110**, 8384 (1999).

[136] I. Røeggen and J. Almlöf, "Interatomic potential for the $X^1\Sigma_g$ state of Be_2", Int. J. Quantum Chem. **60**, 453 (1996).

[137] I. C. Gerber and J. G. Ángyán, "Potential curves for alkaline-earth dimers by density functional theory with long-range correlation corrections", Chem. Phys. Lett. **416**, 375 (2005).

[138] V. F. Lotrich, R. J. Bartlett, and I. Grabowski, "Intermolecular potential energy surfaces of weakly bound dimers computed from ab initio density functional theory: the right answer for the right reason", Chem. Phys. Lett. **405**, 43 (2005).

[139] J. Paier, B. G. Janesko, T. M. Henderson, G. E. Scuseria, A. Grüneis, and G. Kresse, "Hybrid functionals including random phase approximation correlation and second-order screened exchange", J. Chem. Phys. **132**, 094103 (2010).

[140] N. Colonna, M. Hellgren, and S. de Gironcoli, "Molecular bonding with the RPAx: From weak dispersion forces to strong correlation", Phys. Rev. B **93**, 195108 (2016).

[141] B. P. Prascher, D. E. Woon, K. A. Peterson, T. H. Dunning, and A. K. Wilson, "Gaussian basis sets for use in correlated molecular calculations. VII. Valence, core-valence, and scalar relativistic basis sets for Li, Be, Na, and Mg", Theor. Chem. Acc. **128**, 69 (2011).

[142] S. Sharma, T. Yanai, G. H. Booth, C. J. Umrigar, and G. K.-L. Chan, "Spectroscopic accuracy directly from quantum chemistry: Application to ground and excited states of beryllium dimer", J. Chem. Phys. **140**, 104112 (2014).

[143] J. M. Luttinger and J. C. Ward, "Ground-state energy of a many-fermion system. ii", Phys. Rev. **118**, 1417 (1960).

[144] G. Baym and L. P. Kadanoff, "Conservation laws and correlation functions", Phys. Rev. **124**, 287 (1961).

[145] A. Klein, "Perturbation theory for an infinite medium of fermions. ii", Phys. Rev. **121**, 950 (1961).

[146] N. E. Dahlen, R. van Leeuwen, and U. von Barth, "Variational energy functionals of the green function and of the density tested on molecules", Phys. Rev. A **73**, 012511 (2006).

[147] D. Yokoyama, "Molecular orientation in small-molecule organic light-emitting diodes", J. Mater. Chem. **21**, 19187 (2011).

[148] He Guang S., Tan Loon-Seng, Zheng Qingdong, and Prasad Paras N., "Multiphoton Absorbing Materials: Molecular Designs, Characterizations, and Applications", Chem. Rev. **108**, 1245 (2008).

[149] T. Lei, J.-Y. Wang, and J. Pei, "Roles of flexible chains in organic semiconducting materials", Chem. Mater. **26**, 594 (2014).

[150] P. Hohenberg and W. Kohn, "Inhomogeneous electron gas", Phys. Rev. **136**, B864 (1964).

[151] S. J. A. van Gisbergen, J. G. Snijders, and E. J. Baerends, "Time-dependent Density Functional Results for the Dynamic Hyperpolarizability of C_{60}", Phys. Rev. Lett. **78**, 3097 (1997).

[152] S. M. Parker, D. Rappoport, and F. Furche, "Quadratic Response Properties from TDDFT: Trials and Tribulations", J. Chem. Theory Comput. **14**, 807 (2018).

[153] B. Champagne, E. A. Perpéte, S. J. A. van Gisbergen, E.-J. Baerends, J. G. Snijders, C. Soubra-Ghaoui, K. A. Robins, and B. Kirtman, "Assessment of conventional density functional schemes for computing the polarizabilities and hyperpolarizabilities of conjugated oligomers: an ab initio investigation of polyacetylene chains", J. Chem. Phys. **109**, 10489 (1998).

[154] B. Kirtman, S. Bonness, A. Ramirez-Solis, B. Champagne, H. Matsumoto, and H. Sekino, "Calculation of electric dipole (hyper)polarizabilities by long-range-correction scheme in density functional theory: a systematic assessment for polydiacetylene and polybutatriene oligomers", J. Chem. Phys. **128**, 114108 (2008).

[155] S. Nénon, B. Champagne, and M. I. Spassova, "Assessing long-range corrected functionals with physically-adjusted range-separated parameters for calculating the polarizability and the second hyperpolarizability of polydiacetylene and polybutatriene chains", Phys. Chem. Chem. Phys. **16**, 7083 (2014).

[156] M. B. Oviedo, N. V. Ilawe, and B. M. Wong, "Polarizabilities of $\pi-$Conjugated Chains Revisited: Improved Results from Broken-Symmetry Range-Separated DFT and New CCSD(T) Benchmarks", J. Chem. Theory Comput. **12**, 3593 (2016).

[157] R. Zaleśny, M. Medved, S. P. Sitkiewicz, E. Matito, and J. M. Luis, "Can density functional theory be trusted for high-order electric properties? the case of hydrogen-bonded complexes", J. Chem. Theory Comput. **15**, 3570 (2019).

[158] A. J. Garza, N. A. Wazzan, A. M. Asiri, and G. E. Scuseria, "Can short- and middle-range hybrids describe the hyperpolarizabilities of long-range charge-transfer compounds?", J. Phys. Chem. A **118**, 11787 (2014).

[159] F. A. Bulat, A. Toro-Labbé, B. Champagne, B. Kirtman, and W. Yang, "Density-functional theory (hyper)polarizabilities of push-pull $\pi-$conjugated systems: Treatment of exact exchange and role of correlation", J. Chem. Phys. **123**, 014319 (2005).

[160] D. Rappoport and F. Furche, "Property-optimized gaussian basis sets for molecular response calculations", J. Chem. Phys. **133**, 134105 (2010).

[161] D. Bohm and D. Pines, "A Collective Description of Electron Interactions: III. Coulomb Interactions in a Degenerate Electron Gas", Phys. Rev. **92**, 609 (1953).

[162] H. B. Callen and T. A. Welton, "Irreversibility and generalized noise", Phys. Rev. **83**, 34 (1951).

[163] Y. M. Niquet, M. Fuchs, and X. Gonze, "Exchange-correlation potentials in the adiabatic connection fluctuation-dissipation framework", Phys. Rev. A **68**, 032507 (2003).

[164] J. Harl and G. Kresse, "Cohesive energy curves for noble gas solids calculated by adiabatic connection fluctuation-dissipation theory", Phys. Rev. B **77**, 045136 (2008).

[165] H.-V. Nguyen and S. de Gironcoli, "Efficient calculation of exact exchange and rpa correlation energies in the adiabatic-connection fluctuation-dissipation theory", Phys. Rev. B **79**, 205114 (2009).

[166] E. J. Baerends, D. E. Ellis, and P. Ros, "Self-consistent molecular Hartree—Fock—Slater calculations I. The computational procedure", Chem. Phys. **2**, 41 (1973).

[167] B. I. Dunlap, J. W. D. Connolly, and J. R. Sabin, "On some approximations in applications of X-alpha theory", J. Chem. Phys. **71**, 3396 (1979).

[168] K. Eichkorn, O. Treutler, H. Öhm, M. Häser, and R. Ahlrichs, "Auxiliary basis sets to approximate coulomb potentials", Chemical Physics Letters **240**, 283 (1995).

[169] A. Grüneis, M. Marsman, and G. Kresse, "Second-order møller–plesset perturbation theory applied to extended systems. ii. structural and energetic properties", J. Chem. Phys. **133**, 074107 (2010).

[170] H. Eshuis and F. Furche, "A parameter-free density functional that works for noncovalent interactions", J. Phys. Chem. Lett. **2**, 983 (2011).

[171] B. Nguyen, G. P. Chen, M. M. Agee, A. M. Burow, M. Tang, and F. Furche, "Divergence of Many-Body Perturbation Theory for Noncovalent Interactions of Large Molecules", (2019) 10.26434/chemrxiv.11124251.v1.

[172] J. Gauss, "Molecular properties", in *Modern methods and algorithms of quantum chemistry*, edited by J. Grotendorst (John von Neumann Institute for Computing (NIC), 2000), pp. 509–560.

[173] P. Pulay, "Analytical derivative methods in quantum chemistry", in *Advances in chemical physics* (John Wiley and Sons, Ltd, 2007), pp. 241–286.

[174] Y. Yamaguchi and H. F. Schaefer III, "Analytic derivative methods in molecular electronic structure theory: a new dimension to quantum chemistry and its applications to spectroscopy", in *Handbook of high-resolution spectroscopy* (American Cancer Society, 2011).

[175] P. Pulay, "Ab initio calculation of force constants and equilibrium geometries in polyatomic molecules", Mol. Phys. **17**, 197 (1969).

[176] E. Simandiras, R. Amos, and N. Handy, "The analytic evaluation of second-order Møller-plesset (MP2) dipole moment derivatives", Chem. Phys. **114**, 9 (1987).

[177] J. E. Rice and N. C. Handy, "The calculation of frequency-dependent polarizabilities as pseudo-energy derivatives", J. Chem. Phys. **94**, 4959 (1991).

[178] H. Sambe, "Steady states and quasienergies of a quantum-mechanical system in an oscillating field", Phys. Rev. A **7**, 2203 (1973).

[179] O. Christiansen, P. Jørgensen, and C. Hättig, "Response functions from Fourier component variational perturbation theory applied to a time-averaged quasienergy", Int. J. Quantum Chem. **68**, 1 (1998).

[180] V. K. Voora, S. G. Balasubramani, and F. Furche, "Variational generalized Kohn-Sham approach combining the random-phase-approximation and Green's-function methods", Phys. Rev. A **99**, 012518 (2019).

[181] K. R. S. Chandrakumar, T. K. Ghanty, and S. K. Ghosh, "Static dipole polarizability and binding energy of sodium clusters $Na_n(n = 1 - 10)$: A critical assessment of all-electron based post Hartree–Fock and density functional methods", J. Chem. Phys. **120**, 6487 (2004).

[182] U. Hohm, D. Goebel, and S. Grimme, "Experimental and theoretical study of the dipole polarizability of ferrocene $Fe(C_5H_5)_2$", Chem. Phys. Lett. **272**, 328 (1997).

[183] T. Helgaker, P. Jørgensen, and J. Olsen, "Orbital rotations", in *Molecular electronic-structure theory* (John Wiley and Sons, Ltd, 2014) Chap. 3, pp. 80–106.

[184] F. Weigend, M. Häser, H. Patzelt, and R. Ahlrichs, "Ri-mp2: optimized auxiliary basis sets and demonstration of efficiency", Chem. Phys. Lett. **294**, 143 (1998).

[185] M. E. Casida, "Time-dependent density functional response theory for molecules", in *Recent advances in density functional methods* (1995), pp. 155–192.

[186] T. Helgaker, S. Coriani, P. Jørgensen, K. Kristensen, J. Olsen, and K. Ruud, "Recent advances in wave function-based methods of molecular-property calculations", Chem. Rev. **112**, 543 (2012).

[187] H. Weiss, R. Ahlrichs, and M. Häser, "A direct algorithm for self-consistent-field linear response theory and application to c60: excitation energies, oscillator strengths, and frequency-dependent polarizabilities", J. Chem. Phys. **99**, 1262 (1993).

[188] E. R. Davidson, "The iterative calculation of a few of the lowest eigenvalues and corresponding eigenvectors of large real-symmetric matrices", J. Comput. Phys. **17**, 87 (1975).

[189] T. D. Bouman, A. E. Hansen, B. Voigt, and S. Rettrup, "Large-scale RPA calculations of chiroptical properties of organic molecules: Program RPAC", Int. J. Quantum Chem. **23**, 595 (1983).

[190] J. Olsen, H. J. A. Jensen, and P. Jørgensen, "Solution of the large matrix equations which occur in response theory", J. Comput. Phys. **74**, 265 (1988).

[191] A. J. Sadlej, "Molecular electric polarizabilities. Electronic-field-variant (EFV) gaussian basis set for polarizability calculations", Chem. Phys. Lett. **47**, 50 (1977).

[192] A. J. Sadlej and M. Urban, "Medium-size polarized basis sets for high-level-correlated calculations of molecular electric properties: III. Alkali (Li, Na, K, Rb) and alkaline-earth (Be, Mg, Ca, Sr) atoms", J. Mol. Struct. THEOCHEM **234**, 147 (1991).

[193] F. Jensen, "Basis Set Convergence of Nuclear Magnetic Shielding Constants Calculated by Density Functional Methods", J. Chem. Theory Comput. **4**, 719 (2008).

[194] F. Jensen, "The basis set convergence of spin spin coupling constants calculated by density functional methods", J. Chem. Theory Comput. **2**, 1360 (2006).

[195] R. D. Johnson III, ed., *NIST computational chemistry comparison and benchmark database, NIST standard reference database number 101, editor: russell D. Johnson III*, 2019.

[196] D. Hait and M. Head-Gordon, "How accurate are static polarizability predictions from density functional theory? An assessment over 132 species at equilibrium geometry", Phys. Chem. Chem. Phys. **20**, 19800 (2018).

[197] D. Bokhan, D. N. Trubnikov, A. Perera, and R. J. Bartlett, "Explicitly correlated coupled-cluster theory for static polarizabilities", J. Chem. Phys. **145**, 134104 (2016).

[198] S. J. A. van Gisbergen, P. R. T. Schipper, O. V. Gritsenko, E. J. Baerends, J. G. Snijders, B. Champagne, and B. Kirtman, "Electric Field Dependence of the Exchange-Correlation Potential in Molecular Chains", Phys. Rev. Lett. **83**, 694 (1999).

[199] W. G. Aulbur, L. Jönsson, and J. W. Wilkins, "Polarization-dependent density-functional theory and quasiparticle theory: optical response beyond local-density approximations", Phys. Rev. B **54**, 8540 (1996).

[200] P. Mori-Sánchez, Q. Wu, and W. Yang, "Accurate polymer polarizabilities with exact exchange density-functional theory", J. Chem. Phys. **119**, 11001 (2003).

[201] W. Yang and Q. Wu, "Direct Method for Optimized Effective Potentials in Density-Functional Theory", Phys. Rev. Lett. **89**, 143002 (2002).

[202] O. Treutler and R. Ahlrichs, "Efficient molecular numerical integration schemes", J. Chem. Phys. **102**, 346 (1995).

[203] R. Liu, S.-H. Ke, H. U. Baranger, and W. Yang, "Organometallic spintronics: dicobaltocene switch", Nano Lett. **5**, 1959 (2005).

[204] A. Ishii and T. Miyasaka, "A metallocene molecular complex as visible-light absorber for high-voltage organic–inorganic hybrid photovoltaic cells", Chem. Phys. Chem. **15**, 1028 (2014).

[205] D. Goebel and U. Hohm, "Comparative study of the dipole polarizability of the metallocenes $Fe(C_5H_5)_2$, $Ru(C_5H_5)_2$ and $Os(C_5H_5)_2$", J. Chem. Soc., Faraday Trans. **93**, 3467 (1997).

[206] F. N. N. Pansini and F. A. L. de Souza, "Trends in the Spin States and Mean Static Dipole Polarizability of the Group VIIIA Metallocenes", J. Phys. Chem. A **120**, 2771 (2016).

[207] D. Rayane, A. Allouche, E. Benichou, R. Antoine, M. Aubert-Frecon, P. Dugourd, M. Broyer, C. Ristori, F. Chandezon, B. Huber, and C. Guet, "Static electric dipole polarizabilities of alkali clusters", Eur. Phys. J. D **9**, 243 (1999).

[208] W. D. Knight, K. Clemenger, W. A. de Heer, and W. A. Saunders, "Polarizability of alkali clusters", Phys. Rev. B **31**, 2539 (1985).

[209] A. D. Becke, "Density-functional thermochemistry. III. The role of exact exchange", J. Chem. Phys. **98**, 5648 (1993).

[210] D. J. Thouless, "Stability conditions and nuclear rotations in the Hartree-Fock theory", Nucl. Phys. **21**, 225 (1960).

[211] A. Fetter and J. Walecka, *Quantum theory of many-particle systems*, International series in pure and applied physics (McGraw-Hill, 1971).

Appendix A

Intermediates involved in the implementation of GKS-spRPA static polarizabilities

A.1 Zeroth order intermediates

The expressions for the $\boldsymbol{\gamma}$ and $\mathbf{T}$ matrices introduced in Eq. 3.12 may be expressed as

$$\gamma_{ip} = 2\int_{-\infty}^{\infty}\frac{d\omega}{2\pi}\sum_{b}(GB\tilde{Q}B^{T})_{ibpb}, \tag{A.1}$$

$$\gamma_{ap} = 2\int_{-\infty}^{\infty}\frac{d\omega}{2\pi}\sum_{j}(GB\tilde{Q}B^{T})_{jajp}, \tag{A.2}$$

$$T_{ij} = \int_{-\infty}^{\infty}\frac{d\omega}{\pi}\sum_{a}\left(GB\tilde{Q}BG - \omega^{2}\Delta^{-1}GB\tilde{Q}BG\Delta^{-1}\right)_{iaja}, \tag{A.3}$$

$$T_{ab} = \int_{-\infty}^{\infty}\frac{d\omega}{\pi}\sum_{i}\left(GB\tilde{Q}BG - \omega^{2}\Delta^{-1}GB\tilde{Q}BG\Delta^{-1}\right)_{iaib}. \tag{A.4}$$

A.2 Orbital rotations

Starting from a fixed set of orbitals and a reference determinant ($|\Phi\rangle$) any determinant[210] can be written as

$$|\Phi(\hat{\boldsymbol{\kappa}})\rangle = e^{-\hat{\boldsymbol{\kappa}}} |\Phi\rangle \,, \tag{A.5}$$

where the operator $\hat{\boldsymbol{\kappa}}$ can be expressed in terms of the fermion creation and annihilation operators[211] $\hat{C}_p^\dagger,\ \hat{C}_q$ as

$$\hat{\boldsymbol{\kappa}} = \sum_{ia} \left(\kappa_{ia} \hat{C}_i^\dagger \hat{C}_a + \kappa_{ai} \hat{C}_a^\dagger \hat{C}_i \right), \tag{A.6}$$

$$\hat{\boldsymbol{\kappa}}^\dagger = \sum_{ia} \left(\kappa_{ia}^* \hat{C}_a^\dagger \hat{C}_i + \kappa_{ai}^* \hat{C}_i^\dagger \hat{C}_a \right), \tag{A.7}$$

$$\hat{\boldsymbol{\kappa}}^\dagger = -\hat{\boldsymbol{\kappa}} (\text{unitary rotations}), \tag{A.8}$$

$$\kappa_{ia}^* = -\kappa_{ai} \quad \text{and} \quad \kappa_{ai}^* = -\kappa_{ia}. \tag{A.9}$$

Using all these results, for real orbital rotation parameters κ_{ia}, the orbital rotation operator may be expressed as

$$\hat{\boldsymbol{\kappa}} = \sum_{ia} \kappa_{ia} \left(\hat{C}_i^\dagger \hat{C}_a - \hat{C}_a^\dagger \hat{C}_i \right). \tag{A.10}$$

A.3 GKS-spRPA algorithm

The self-consistent scheme of the GKS-spRPA is depicted in this flowchart

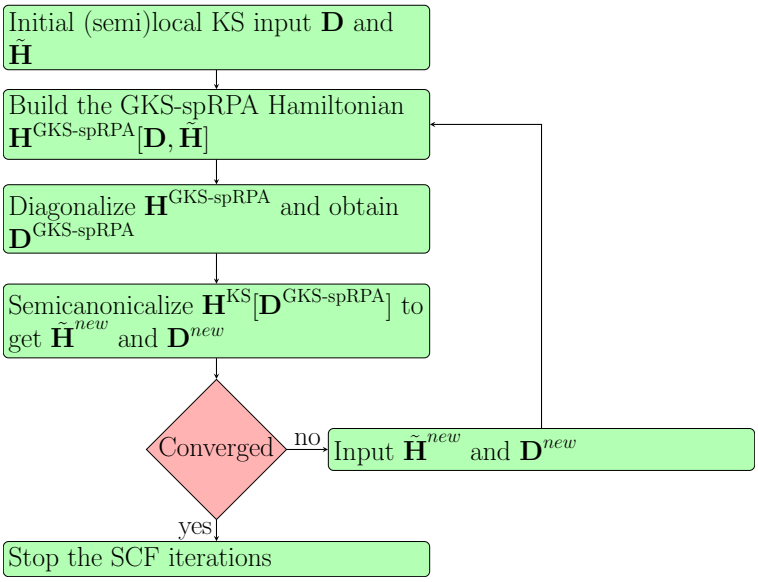

Figure A.1: Flowchart of the GKS-spRPA scheme.

A.4 First order intermediates

In this section we discuss the definitions and forms of certain important first-order matrices necessary for calculating second-order properties within the GKS-spRPA. First derivatives with respect to internal perturbations such as the orbital rotations[47] are defined as

$$A^{(1)}_{pq} = \sum_{ia} \frac{\partial A_{pq}}{\kappa_{ia}} \kappa_{ia}. \tag{A.11}$$

Since the GKS-spRPA energy is invariant to occupied-occupied (oo) and virtual-virtual (vv) orbital rotations, the only non-zero blocks of the orbital rotation matrix $\boldsymbol{\kappa}$ are κ_{ov}. First derivatives with respect to the external electric field perturbations (say E_x, the electric field along the $\hat{x}$ direction) are obtained as

$$A^{x}_{pq} = \left(\frac{dA_{pq}}{dE_x}\right)_{\vec{E}=\vec{0}} = \left(\frac{\partial A_{pq}}{\partial E_x}\right)_{\vec{E}=\vec{0}} + \sum_{rs} \frac{\partial A_{pq}}{\partial F_{rs}} \left(\frac{\partial F_{rs}}{\partial E_x}\right)_{\vec{E}=\vec{0}}. \tag{A.12}$$

where $\boldsymbol{F}$ is the KS semilocal Fock matrix and $\left(\frac{\partial F_{rs}}{\partial E_x}\right)_{\vec{E}=\vec{0}} = \mu^x_{rs}$, the matrix elements of the dipole moment operator.

A.4.1 Three center electron repulsion integrals

First order three electron integrals in the RI basis [166–168] can be expressed as

$$B^{(1)}_{ia\mathcal{P}} = \sum_b B_{ba\mathcal{P}}\kappa_{ib} - \sum_j B_{ij\mathcal{P}}\kappa_{ja}. \tag{A.13}$$

A.4.2 KS polarization propagator matrix

The KS polarization propagator matrix in the noncanonical basis can be expressed as

$$\mathbf{G} = \boldsymbol{\Delta}(\boldsymbol{\Delta}^2 + \omega^2\mathbb{1})^{-1}. \tag{A.14}$$

The first order $\mathbf{G}$ matrix can be derived as

$$\mathbf{G}^{(1)} = \boldsymbol{\Delta}^{(1)}(\boldsymbol{\Delta}^2 + \omega^2\mathbb{1})^{-1} - \boldsymbol{\Delta}(\boldsymbol{\Delta}^2 + \omega^2\mathbb{1})^{-1}(\boldsymbol{\Delta}^{(1)}\boldsymbol{\Delta} + \boldsymbol{\Delta}\boldsymbol{\Delta}^{(1)})(\boldsymbol{\Delta}^2 + \omega^2\mathbb{1})^{-1}, \tag{A.15}$$

$$= \omega^2\mathbf{G}\boldsymbol{\Delta}^{-1}\boldsymbol{\Delta}^{(1)}\boldsymbol{\Delta}^{-1}\mathbf{G} - \mathbf{G}\boldsymbol{\Delta}^{(1)}\mathbf{G}. \tag{A.16}$$

A.4.3 KS Semilocal Fock matrix

The first-order KS semilocal Fock matrix has the form

$$F^{(1)}_{pq} = \sum_r \kappa_{pr}F_{rq} + \sum_j F_{pr}\kappa_{rq} + \mathrm{H}^{+}_{pq}[\boldsymbol{\kappa}] \tag{A.17}$$

where the symmetric super-matrix $\mathbf{H}^{+}$ is given by

$$\mathbf{H}^{+} = \frac{\delta\mathbf{V}^{\mathrm{HXC}}}{\delta\mathbf{D}^{T}}, \tag{A.18}$$

and [] denotes its contraction with a matrix X, which is defined as

$$\mathrm{H}^{+}_{pq}[X] = \sum_{rs} \mathrm{H}^{+}_{pqrs} X_{rs}. \tag{A.19}$$

A.4.4 Q matrix

The definitions of the $\mathbf{Q}$ and $\tilde{\mathbf{Q}}$ matrices are

$$\mathrm{Q}_{\mathcal{PQ}} = \sum_{iajb} B_{\mathcal{P}ia} \mathrm{G}_{iajb} B_{jb\mathcal{Q}}, \tag{A.20}$$

$$\tilde{\mathrm{Q}}_{\mathcal{PQ}} = (\mathbb{1} + \mathrm{Q})^{-1}_{\mathcal{PQ}} - \mathbb{1}_{\mathcal{PQ}}, \tag{A.21}$$

where $\mathbb{1}$ is the identity matrix. The first derivatives of these matrices are

$$\mathbf{Q}^{(1)} = \boldsymbol{B}^{(1)}\mathbf{G}\boldsymbol{B} + \boldsymbol{B}\mathbf{G}^{(1)}\boldsymbol{B} + \boldsymbol{B}\mathbf{G}\boldsymbol{B}^{(1)}, \tag{A.22}$$

where Eqs. A.13 and A.16 can be used to evaluate this.

$$\tilde{\mathbf{Q}}^{(1)} = -(\mathbb{1} + \mathbf{Q})^{-1}\mathbf{Q}^{(1)}(\mathbb{1} + \mathbf{Q})^{-1} \tag{A.23}$$

A.4.5 First-order GKS-spRPA Fock matrix

The occupied-virtual block of the GKS-spRPA Fock matrix [180] is given by

$$F^{\text{GKS-spRPA}}_{ia} = F^{\text{HF}}_{ia} + \gamma_{ai} - \gamma_{ia} + \mathrm{H}^{+}_{ia}[\mathbf{T}] + \sum_{j} \mathrm{T}_{ij} F^{\text{KS}}_{ja} + \sum_{b} F^{\text{KS}}_{ib} \mathrm{T}_{ba}. \tag{A.24}$$

In the following the expressions for the first derivatives of γ_{ai}, T_{ij} and $\mathrm{H}^{+}_{ia}[\mathbf{T}]$ are provided. These derivatives are expressed in terms of the first-order matrices derived in Eqns. A.13,

A.16, A.17, A.20 and A.21.

$$\gamma_{ai}^{(1)} = \int_{-\infty}^{\infty} \frac{d\omega}{2\pi} \sum_{\mathcal{P}j} \left(B_{ja\mathcal{P}}^{(1)} \left(\mathbf{G}\boldsymbol{B}\tilde{\mathbf{Q}} \right)_{\mathcal{P}ji} + B_{ja\mathcal{P}} \left(\mathbf{G}\boldsymbol{B}\tilde{\mathbf{Q}} \right)_{\mathcal{P}ji}^{(1)} \right). \tag{A.25}$$

$$\begin{aligned} \mathrm{T}_{ij}^{(1)} = \sum_a \int \frac{d\omega}{2\pi} \Big[& \quad \left(\mathbf{G}\boldsymbol{B}\tilde{\mathbf{Q}} \right)^{(1)} \boldsymbol{B}\mathbf{G} - \omega^2 \boldsymbol{\Delta}^{-1} \left(\mathbf{G}\boldsymbol{B}\tilde{\mathbf{Q}} \right)^{(1)} \boldsymbol{B}\mathbf{G}\boldsymbol{\Delta}^{-1} + \left(\mathbf{G}\boldsymbol{B}\tilde{\mathbf{Q}} \right) (\boldsymbol{B}\mathbf{G})^{(1)} \\ & - \omega^2 \boldsymbol{\Delta}^{-1} \mathbf{G}\boldsymbol{B}\tilde{\mathbf{Q}} \, (\boldsymbol{B}\mathbf{G})^{(1)} \, \boldsymbol{\Delta}^{-1} - \left(\boldsymbol{\Delta}^{-1} \boldsymbol{\Delta}^{(1)} \hat{\mathbf{G}} \boldsymbol{B}\tilde{\mathbf{Q}} \boldsymbol{B}\mathbf{G}\boldsymbol{\Delta}^{-1} + Transpose \right) \Big]_{iaja} \end{aligned} \tag{A.26}$$

$$\begin{aligned} \left(\mathrm{H}_{ia}^{+}[\mathbf{T}] \right)^{(1)} = \sum_{jb} \frac{\partial \left(\mathrm{H}_{ia}^{+}[\mathbf{T}] \right)}{\partial \kappa_{jb}} \kappa_{jb} = & \left(\sum_b \kappa_{ib} \mathrm{H}_{ba}^{+}[\mathbf{T}] - \sum_j \mathrm{H}_{ij}^{+}[\mathbf{T}] \kappa_{ja} \right) \\ & + \sum_{\mu\nu\gamma\delta jb} \frac{\partial \mathrm{H}_{ia\mu\nu}^{+}}{\partial \mathrm{D}_{\gamma\delta}} \mathrm{T}_{\mu\nu} \frac{\partial \mathrm{D}_{\gamma\delta}}{\partial \kappa_{jb}} \kappa_{jb} + \sum_{\mu\nu jb} \mathrm{H}_{ia\mu\nu}^{+} \frac{\partial \mathrm{T}_{\mu\nu}}{\partial \kappa_{jb}} \kappa_{jb}. \end{aligned} \tag{A.27}$$

In the AO basis this can be expressed more compactly as

$$\left(\mathrm{H}_{\mu\nu}^{+}[\mathbf{T}] \right)^{(1)} = \mathrm{G}_{\mu\nu}^{+}[\mathbf{T}, \boldsymbol{\kappa}] + \mathrm{H}_{\mu\nu}^{+} \left[\mathbf{T}^{(1)} \right], \tag{A.28}$$

where the hyper-kernel $\mathbf{G}^{+}$ is defined as

$$\mathrm{G}_{\mu\nu\kappa\lambda\delta\chi}^{+} = \frac{\delta \mathrm{H}_{\mu\nu\kappa\lambda}^{+}}{\delta \mathrm{D}_{\delta\chi}}. \tag{A.29}$$